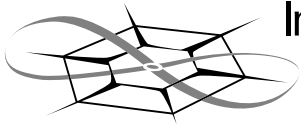


The University of Kansas



**Information and
Telecommunication
Technology Center**

Technical Report

**The Design and Development of a Hybrid RF/Laser
Radar System for Measuring Changes in
Ice Surface Elevation at Arctic Regions**

Christopher T. Allen and Yanki Cobanoglu

ITTC-RSL-FY2002-TR-18680-02

May 2002

Project Sponsor:
Instrument Incubator Program, NRA-98-OES-05
NASA, Langley Research Center

Copyright © 2002:
The University of Kansas
2335 Irving Hill Road, Lawrence, KS 66045-7612
All rights reserved.

ABSTRACT

Satellites carrying laser radars for measuring ice sheet surface elevation, and aerosol characteristics are will be launched in the next few years. To achieve the necessary range accuracy and sensitivity, laser radars on these satellites will use short-duration, high peak power transmit pulses. These laser radars must operate with a low-pulse repetition frequency (PRF) due to the high peak transmit power. The low PRF will cause less dense sampling along the satellite track. The high peak power operation results in limited laser radar lifetime.

To solve the limitation of using high peak transmit power, we have developed a hybrid RF/Laser radar that uses lower peak transmit power and higher PRF. RF pulse compression is used to improve system performance further. Receiver sensitivities of less than -90 dBm have been demonstrated by applying heterodyne detection and RF pulse compression. Compared to laser radars like GLAS and MOLA, this sensor requires a lower peak transmit power while providing more dense sampling of data from target.

Manmade and natural extended-target range measurements have been made and the results are presented.

The experiment and simulation results presented support the feasibility of a satellite-based altimeter (at a 600 km altitude), capable of making more than 4000 range measurements per second with 10 cm range accuracy using less than 10 W peak transmit power.

Table of Contents

Chapter 1 – Introduction	1
1.1 Science Motivation and Objectives	1
1.2 System Overview	2
1.3 NASA & KU RSL Objectives and Overview of Report	3
Chapter 2 – Theory	4
2.1 Introduction	4
2.2 Range Accuracy	4
2.3 Radar Range Equation	6
2.3-1 Numerical Example	10
2.4 Coherent Detection	11
2.5 Pulse Compression	14
2.6 Coherent Integration	17
2.7 Conclusion	18
Chapter 3 – System Design	19
3.1 Introduction	19
3.2 System Block Diagram	19
3.3 How the System Works	20
3.4 Signal Processing	27
Chapter 4 – Simulations	28
4.1 Introduction	28

4.2	System Parameter & Block Diagram	29
4.3	Effects of Coherent Integrations on Output SNR of the System	37
4.4	The Effects of Varying Modulation Index on the Minimum Detectable Optical Input Power for the System	38
4.5	The Effects of varying NEP on the minimum detectable optical input power for the system	40
4.6	The Effects of varying local oscillator, P_{lo} , on the minimum detectable optical input power for the system	42
4.7	Conclusion	44
Chapter 5– System Prototype and Experiment Results		45
5.1	Introduction	45
5.2	System Block Diagram	45
5.3	The Transmitter.....	47
5.3-1	The Waveform Generator	47
5.3-2	The RF Section of the Transmitter	47
	a) Oscillator	47
	b) Low-pass Filter	47
	c) Power Splitter	48
	d) RF Amplifier	48
5.3-3	The Optical Section of the Transmitter	48
	a) Laser Source	48
	b) Acousto-optic Modulator	48
	c) Mach-Zehnder Modulator	48
	d) Optical-fiber Amplifier	48

e) Transmit telescope	49
5.4 The Receiver	49
5.4-1 The Optical Section of the Receiver	49
a) Receive Telescope	49
b) Coherent Receiver	49
5.4-2 The RF Section of the Receiver	50
a) RF Amplifiers	50
b) 3 GHz Oscillator	50
c) RF Mixers	50
d) Bandpass Filter	50
e) Envelope Detector	50
f) Low-pass Filters	51
5.5 The Signal Processing Section	51
5.5-1 The Data Acquisition Module	51
5.5-2 The Signal Processing and Display Module	51
5.6 Experiment Results	52
5.6-1 Results of the experiment to see the effects of changing the pulse width of the signal used	52
5.6-2 Results of the Experiment to See the Effects of Changing the Number of Coherent Integrations on Output SNR and on Minimum Detectable Signal	53
5.6-3 Results of the Experiment to See the Relationship Between Input Optical Signal and Output SNR	55

5.6-4 Min. Detectable Optical Input Signal Power Experiment	56
5.7 Conclusions	59
Chapter 6 – Other System Configurations	60
6.1 Introduction	60
6.2 Homodyne versus Heterodyne Detection	60
6.3 Inphase-Quadrature with Direct Down Conversion	62
Chapter 7 – Conclusion and Future Recommendations	69
References	71
Appendix	72
Appendix A – The Matlab Program Used for Running Simulations to	
Predict System performance	

73

CHAPTER 1

Introduction

1.1 Science Motivation and Objectives

The University of Kansas has been participating in projects determining the mass balance of ice sheets and its contribution to global sea level. An increase of 2° Celsius in Earth's temperature is expected from 1990 to the end of year 2100, even with a minimum amount of greenhouse gas emissions [1]. Scientific evidence also suggests that the Earth's average sea level will rise by about 2 mm per year [2]. If the increase in Earth temperature and sea level continues, some low-lying regions of the world might be flooded and places inhabited by certain species might diminish or disappear, causing these species to become extinct.

These and many other important effects of global climate change demand interest from the research community. The research done to better understand global climate change will provide us with information about trends of the past and present. This will, in turn, help us predict and be prepared for possible changes on both regional and global scales.

One way to monitor the trends of global climate change is to observe the changes in elevation of the ice sheet in the arctic regions of the world. The elevation of these ice sheets is affected by the trends for ice accumulation, ice flow, surface slope, etc.

Advances in satellite instruments and other related technologies have led to remote sensing being an effective tool for observing these changes.

1.2 System Overview

To observe the changes in global climate and to measure vegetation characteristics, and aerosol characteristics, NASA will launch several satellites with laser radars (LIDARs) on board. One of these missions is Geoscience Laser Altimeter System (GLAS). To obtain the necessary resolution and detection sensitivity, GLAS will use short-duration, high-peak power pulses. The use of high-peak power pulses requires high-current power supplies for transmitters, so laser sources used will have limited lifetime. This system also requires the use of low-pulse repetition frequencies (PRFs), which will cause less dense sampling of targets.

The LIDAR that will be presented here is designed to have a higher PRF and lower peak power requirements than the LIDARs to be used in GLAS. When this design is used, the lower peak power requirements will increase the lifetime of the laser sources, and the increased PRF will enable more dense sampling of data. The design is a hybrid of fiber-optic and RF technologies. Some of the advantages of using laser radar technologies are the use of smaller apertures than comparable microwave radars and the range precision obtained from the bandwidth of laser radars.

To further improve the performance of the system, the principles of coherent detection, RF pulse compression and digital signal processing techniques are employed. The wavelength used is 1319 nm, which is different than the 1550 nm wavelength that has been widely used in the fiber optic community. The wavelength is chosen to be 1319 nm not only to improve the sensitivity to snow and ice but also to continue exploiting the commercially available fiber-optic components such as distributed-feedback (DFB) lasers, modulators, and praseodymium-doped fluoride fiber amplifiers (PDFFAs) [3].

1.3 NASA and University of Kansas Remote Sensing Lab (RSL) Objectives and Overview of the Report

The primary objective of this project is to develop a LIDAR that uses less power and has a longer laser lifetime than previously available LIDARs currently used for ice sheet elevation observation. A lower peak power and longer pulse will be used to increase the lifetime of the lasers on board and PRF will be increased to allow more dense sampling.

This report documents the progress of the project and steps taken to achieve the goal given above. It is divided into seven chapters. The first chapter is the introduction and provides an overview of reasons behind the observation of ice sheet elevation change, objectives to be achieved and a brief explanation of the system improvements. The second chapter is the theory section and provides theoretical background for the concepts employed in the project. It also includes step-by-step analytical explanation of the concepts and formulaic analysis of the signals used in the system. Chapter 3 deals with detailed description of our system.

Chapter 4 presents the simulations we did to predict the behavior of the system under different conditions or with different parameters to find the best way to bring the Lidar into reality. Chapter 5 presents our experiments with the laboratory setup to verify the results of the simulations and help better understand the performance of the system. Chapter 6 includes the discussion of other system configurations tested, and Chapter 7 presents the conclusions.

CHAPTER 2

Theory

2.1 Introduction

Laser radars employ techniques developed for conventional radars at very short wavelengths. The use of shorter wavelengths enables the laser radars to achieve more precise resolution and higher accuracy than microwave radars. However, their use is generally restricted to lower parts of the atmosphere. To be able to achieve the elevation needed for our project, while still providing the necessary range accuracy, we will employ pulse compression, coherent integration and coherent detection techniques.

Below are sections that include a block diagram of the system used, explanation of the abbreviations used in the formulas, as well as the explanation the techniques employed for improving the system performance.

2.2 Range Accuracy

The laser radar will be designed to achieve the proposed improvements of size and power consumption and sensor flexibility. During the design of the laser radar system, the key parameter is range accuracy. Range accuracy is the expected error in the true range to the target. In general, the required range accuracy is determined by the application. For ice sheet elevation monitoring, the glaciological community requires 10 cm.

The range accuracy is affected by two parameters: effective bandwidth and signal-to-noise ratio (SNR)[4]. This is evident from the following representation for range accuracy: [4]

$$\sigma_R = \frac{c}{2 B \sqrt{2 SNR}} \quad [2.2-1]$$

where

σ_R = RMS (root-mean-square) error in range measurement [m]

SNR = signal-to-noise ratio at the output of the system

c = speed of light [m/s]

B = pulse bandwidth [Hz]

As seen from this equation, increasing the effective bandwidth or improving the signal-to-noise ratio reduces the error in range measurement, thus improving the range accuracy of the system. The bandwidth of our system is set at the same value as the one used for the Geoscience Laser Altimeter System (GLAS) system. It can be increased further to obtain better range accuracy, but this increase might bring some unwanted extra costs to the system. When the bandwidth of the system is increased, this might also increase the processing time of the collected data on board or require more bandwidth to send it to the Earth control point. Because of this extra cost, a reasonable value is chosen for the bandwidth to keep the bandwidth cost low. (A reasonable level is also needed since [2.2-1] is valid for SNRs higher than 10.) However, the SNR of the system can be improved by employing methods like pulse compression, coherent integration and coherent detection techniques.

To predict the SNR at the photo diode output, we will use radar range equation.

2.3 Radar Range Equation

From the radar range equation we can determine the received power and the SNR for a given system configuration. The equation presented has its basis from the microwave radar range equation since principles of electromagnetic propagation are still applicable.

$$P_r = \frac{P_t G_t}{4\pi R^2} \frac{\sigma G_a}{4\pi R^2} A_{ap} \eta_{sys} \quad [2.3-1]$$

where

P_r	=	received optical power [W]
P_t	=	transmitter optical power [W]
G_t	=	transmitter antenna gain
σ	=	effective target cross section [m ²]
R	=	range to the target [m]
D	=	receive aperture diameter [m]
G_a	=	optical amplifier gain
η_{sys}	=	system transmission factor
A_{ap}	=	effective receive aperture area $(\frac{\pi D^2}{4})$ [m ²]

The transmitter antenna gain is found using the equation

$$G_t = 4\pi / \theta_r^2 \quad [2.3-2]$$

where θ_r^2 is the solid angle of the transmitter beamwidth in steradians [sr][4]. Since the equation for G_t is only valid for far-field applications, the equation needs to be modified for applications in the near field. Our ice sheet elevation measurement project is one that operates in the near field, so the necessary adjustments need to be made to obtain a correct model from the radar range equation. The near field is defined as follows:

$$\text{Range to the target, } R < \frac{2D^2}{\lambda}$$

where

$$\lambda = \text{the wavelength [m]}$$

With the wavelength used in our design, the system operates in the near field. The beamwidth should be modified as follows for the near-field applications [4]:

$$\theta_r^2 = \left[\left(\frac{K_a D}{R} \right)^2 + \left(\frac{K_a \lambda}{D} \right)^2 \right] \quad [2.3-3]$$

where

K_a = aperture illumination constant (a constant used to illustrate the difference between radar and various optical beamwidth definitions [4])

The effective target cross section depends on the target reflectivity and illuminated target area. Its representation is as follows [4]:

$$\sigma = \frac{4\pi}{\Omega} \rho_t A_{ill} \quad [2.3-4]$$

where

Ω = scattering solid angle of target [sr]

ρ_t = target reflectivity

A_{ill} = illuminated target area [m^2]

This formula shows that as the target reflectivity gets bigger, the effective cross section increases, which also increases the received power,. For natural extended area targets, we can assume Lambertian scattering, where the scattering occurs uniformly in all directions [5]. The equation for the effective target cross section is reduced to the form below for Lambertian targets, since the value for Ω is replaced with the value for the standard scattering diffuse target having a solid angle of π steradians [4]:

$$\sigma = 4\rho_t A_{ill} \quad [2.3-5]$$

Since the target for our system is the ice sheet, it will intercept the entire beam from the transmitter. This kind of target is called an extended target and it has an illuminated area, A_{ill} , with a range-square dependency, shown below[4]:

$$A_{ill} = \frac{\pi R^2 \theta_r^2}{4} \quad [2.3-6]$$

While calculating the received power to the system, we should also take the limitations of the equipment into account. This is entered into the radar range equation with the η_{sys} parameter.

The optical signal is incident of the photo diode to be converted to an electrical signal. The output current obtained from a photo diode with incoherent (direct) detection may be expressed as [4] :

$$i_{sig} = \mathfrak{R} E_{sig}^2 = \mathfrak{R} P_r \quad [2.3-7]$$

where

\mathfrak{R} = detector responsivity [A/W]

E_{sig} = electric field incident on the detector [V/m]

Responsivity is a measure of the sensitivity of the photo diode and is the ratio of the current output of the diode, I_{out} , to the incident optical power, P_{in} , given in the following formula [6]:

$$\mathfrak{R} = I_{out} / P_{in} \quad [2.3-8]$$

To obtain an expression for SNR we need to obtain the signal power in the electrical domain. The following expression transforms the optical domain signal power, P_r , into the electrical domain signal power, P_{sig} .

$$P_{sig} = \mathfrak{R}^2 P_r^2 \quad [2.3-9]$$

When the signal power in electrical domain is obtained, the expression for SNR at the output of the photo diode can be obtained:

$$SNR = P_{sig} / P_n \quad [2.3-10]$$

where

P_{sig} = signal power in the electrical domain [W]

P_n = noise power in the electrical domain [W]

As seen from [2.3-10], the value for this received signal power in the optical domain, P_r , affects signal power in the electrical domain, which in turn affects SNR and range accuracy. This SNR is the ratio of the signal power P_{sig} and the noise power P_n measured at the output of the photo diode (at point A), as shown in Figure 2.3-1 below.

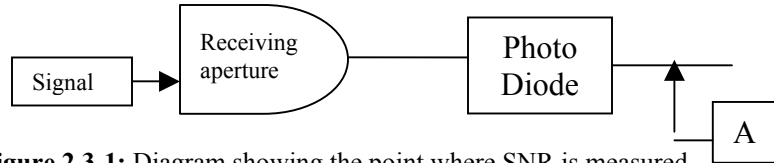


Figure 2.3-1: Diagram showing the point where SNR is measured.

The noise is assumed to come from the photo diode. It is assumed that the noise power, P_n , is due to thermal and shot noise produced in the photo diode. The thermal noise is modeled using the following formula:

$$P_{n-th} = \mathfrak{R}^2 NEP^2 B_{rec} \quad [2.3-11]$$

where

$$NEP = \text{noise equivalent power [W/}\sqrt{\text{Hz}} \text{]}$$

$$B_{rec} = \text{receiver bandwidth [Hz]}$$

Noise equivalent power, NEP, is given as a performance parameter for photo diodes and is defined as the optical power incident on the diode that will make the SNR equal to 1 for a fixed thermal noise level.

Shot noise is associated with quantization of light energy into photons. The value for shot noise power, P_{n-sh} , can be obtained using the following formula:

$$P_{n-sh} = 2qI B_{rec} \quad [2.3-12]$$

where

$$q = \text{electron charge [} 1.6 \times 10^{-19} \text{ C]}$$

$$I = \text{average output current of the photo diode [A]}$$

The output current has two main components, which are I_{incident} and I_{dark} . The incident current is caused by the incoming photons hitting the photo diode, while the dark current is the output of the photo diode with no input illumination.

We can now combine representations for noise power and signal power, to obtain a complete formula for SNR with incoherent detection:

$$\text{SNR}_{\text{incoh}} = \frac{\mathfrak{R}^2 P_r^2}{\mathfrak{R}^2 \text{NEP}^2 B_{\text{rec}} + 2q I_{\text{Brec}}} \quad [2.3-13]$$

2.3-1 Numerical Example: Next we will look at a numerical example to obtain a numerical value for the SNR with the parameters chosen to represent the system that will be built. The system parameter values for a Lambertian target are as follows.

System Parameters

$$P_t = 10 \text{ mW}$$

$$\lambda = 1310 \text{ nm}$$

$$D = 1 \text{ m}$$

$$R = 600 \text{ km}$$

$$B_{\text{rec}} = 800 \text{ MHz}$$

$$\eta_{\text{sys}} = 0.3$$

$$\rho_t = 0.5$$

$$\mathfrak{R} = 0.7 \text{ A/W}$$

$$\text{NEP} = 2.4 \times 10^{-11} \text{ W}/\sqrt{\text{Hz}}$$

$$G_a = 23 \text{ dB}$$

Calculated Parameters

$$G_t = 7.323 \times 10^{12}$$

$$A_{\text{ill}} = 0.4852$$

$$P_r = 0.165 \text{ pW}$$

$$I_{\text{incident}} = 1 \text{ } \mu\text{A}$$

$$I_{\text{dark}} = 1 \text{ nA}$$

The value for signal power, P_{sig} , turns out to be $1.33 \times 10^{-26} \text{ W}$. The value for the thermal noise power, $P_{\text{n-th}}$, is $2.26 \times 10^{-13} \text{ W}$. The value for the shot noise power, $P_{\text{n-sh}}$, is

2.56×10^{-16} W. Since the shot noise term is small compared to the thermal noise, the noise power is assumed to be caused only by thermal noise ($P_n = P_{n-th}$). These values for signal and noise power give an $SNR = 5.88 \times 10^{-14}$, which is about -132 dB.

This value of SNR is too low to give the range accuracy and target detection we are looking for. Since this is the case, methods for improving the receiver sensitivity will be explored. These methods include coherent detection, pulse compression and coherent integration, which will be employed to increase the sensitivity of our system.

2.4 Coherent Detection

The coherent detection scheme is similar to the incoherent technique with one exception; in this scheme an optical local oscillator [LO] signal is coupled to the photo diode during the detection process. When the incoming optical signal reaches the receiver, it is mixed with this local oscillator signal and then passed to the photo diode. A simple diagram for a coherent system is shown below in Figure 2.4-1.

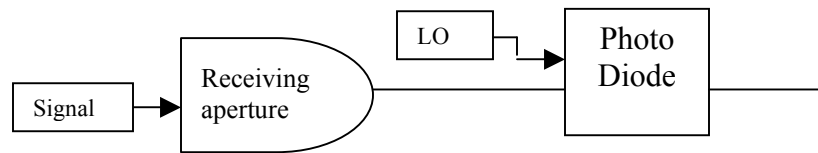


Figure 2.4-1: Diagram showing the addition of the LO.

Since the detection process includes a local oscillator, the expression for the signal current out of the photo diode changes. For the coherent detection scheme, the output current is as follows:

$$i_{sig} = \Re(\vec{E}_r + \vec{E}_{lo})^2 = \Re(\vec{E}_r^2 + \vec{E}_{lo}^2 + 2\vec{E}_r \bullet \vec{E}_{lo}) \quad [2.4-1]$$

where

E_{lo} = electric field vector due to the local oscillator

E_r = electric field vector due to the received signal

The expression for output current in terms of power instead of electric fields would be:

$$i_{sig} = \Re P_r + \Re P_{lo} + 2 \Re \sqrt{P_r P_{lo}} \cos(\gamma/2) \cos[(\omega_{sig} - \omega_{lo})t + \phi] \quad [2.4-2]$$

where

ω_{sig} = signal frequency [radians/s]

ω_{lo} = local oscillator frequency [radians/s]

ϕ = phase difference between signal and LO [radians]

P_{lo} = local oscillator power [W]

γ = polarization difference between received signal and LO

The expression above contains three terms. Only the third one is of interest for a coherent detection scheme. The first term is from direct detection and it appears at baseband. It is at a part of the spectrum that is outside the frequency range of interest and is filtered out. The second term appears at DC. The third term appears at a frequency $\omega_{if} = \omega_{sig} - \omega_{lo}$ and it contains the multiplication of the signal and the LO terms. It is this multiplication that is desired from coherent detection, and the signals outside the desired part of the spectrum are filtered out. So, only looking at the term of interest gives the following expression for the i_{sig} :

$$i_{sig} = \Re \sqrt{P_r P_{lo}} \cos(\gamma/2) \cos[(\omega_{sig} - \omega_{lo})t + \phi] \quad [2.4-3]$$

The desired cross term is the multiplication of the electric fields of the signal and the local oscillator, which gives the following simplified expression:

$$i_{sig} = 2 \Re(\vec{E}_r \cdot \vec{E}_w) \quad [2.4-4]$$

This is equivalent to the expression obtained from [2.4-3]. (The use of dot product is necessary to account for the polarization difference between the signal and the LO.)

To obtain the maximum value for the output signal current, the value for γ is optimized. This term is included in [2.4-3] to account for the polarization difference between the signal and local oscillator electric fields. This polarization difference accounts for the degree of copolarization of the two signals. When they are not copolarized, the obtained signal power decreases.

As seen from [2.4-3], the local oscillator power affects the signal current and, in turn, signal power, P_{sig} . The SNR equation for coherent detection is as follows:

$$SNR_{coh} = \frac{\mathfrak{R}^2 P_{lo} P_r}{P_{n-th} + P_{n-sh}} \quad [2.4-5]$$

Now that we obtained an expression for SNR for coherent detection, we can look at a numerical example to see the improvement in SNR compared to the incoherent detection system.

If $P_{lo} = 1$ mW and all other parameter values are same as they were for the incoherent detection scheme, the new value for electrical signal power, P_{sig} , is 8.10×10^{-17} W, an improvement of about 98 dB. The noise term also increases, however, due to the increase of shot noise. Shot noise is higher since $I_{incident}$ is higher. The increase of $I_{incident}$ is due to the contribution from the LO current. The new shot noise value is 2.56×10^{-13} W, while the value for the thermal noise power stays same at, P_{n-th} , is 2.26×10^{-13} W. This new value for signal power and the total noise power of 4.82×10^{-13} W gives an SNR of about -38 dB. This is an improvement of 94 dB compared to incoherent detection. With this improvement, we will need an increase of 48 dB of signal power to obtain the necessary range accuracy for our system.

2.5 Pulse Compression

Pulse compression is a technique widely used in radar systems to improve sensitivity. In our case the pulse compression process has a long-duration pulse, low-peak-power, modulated transmit waveform to attain the detection and range resolution comparable to that of a short-pulse, high-peak-power system.

One pulse compression method uses chirped signals. A chirp pulse-compressed system has a sinusoidal pulse with a long duration, T , and an instantaneous frequency varying linearly with time. In other words, the pulse used is a chirp-modulated signal. Figure 2.5-1 below illustrates this concept.

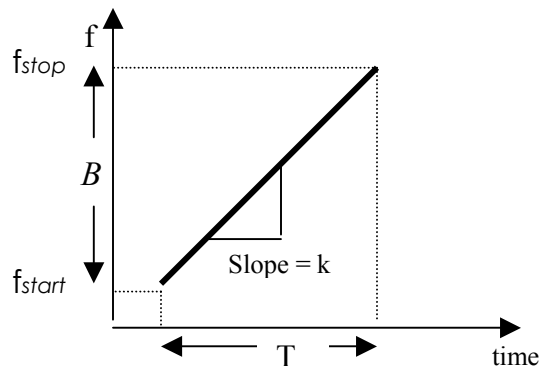


Figure 2.5-1: Illustration of the concept of using a chirp signal.

The slope of the line, k , is known as the chirp rate and is the ratio of the system bandwidth, B , to the system pulsewidth, T .

The following expression is a mathematical description of the chirp signal:

$$S_{\text{chirp}} = A_c \sin \left(2\pi \left(f_{\text{start}} t + \frac{k}{2} t^2 + \phi_{\text{st}} \right) \right) \quad \text{for } 0 \leq t \leq T \quad [2.5-1]$$

where

A_c = amplitude of the chirp [V]

f_{start} = starting frequency of the chirp [Hz]

ϕ_{st} = starting phase of the waveform [radians]

This chirp signal is used to amplitude modulate the transmitted signal. The following expression gives a mathematical description of the chirp-modulated signal:

$$S_{tx} = A_{tx} (1 + \mu S_{chirp}) \sin(2\pi f_{car} t + \phi_{optical}) \quad [2.5-2]$$

where

A_{tx} = amplitude of the transmitted signal [V]

μ = modulation index

f_{car} = carrier frequency [Hz]

$\phi_{optical}$ = phase of the optical signal [radians]

The range for the modulation index is between 0 and 1. In our case, a value close to 1 is chosen to ensure maximum power transmission.

After the signal is transmitted, it reaches the target and is backscattered. A portion of this backscattered signal, S_{rx} , is captured at the receiving aperture of the system. The following figure shows a graphical description of the received signal.

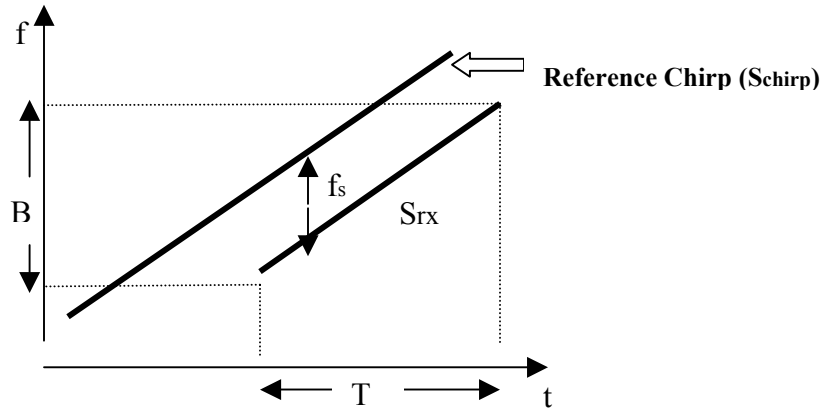


Figure 2.5-2: Graphical representation of reference and received signal.

Since we have a nadir-looking radar, all the received energy comes from a target at fixed range. This received signal is shown in figure 2.5-2 as signal S_{rx} . The difference in frequency between S_{rx} and the reference chirp, f_s , is the frequency that gives the range to the target. After several processing steps (which will be explained in Chapter 3), the received signal is multiplied with the S_{chirp} . This multiplication is called dechirping.

After dechirping, we low-pass filter the dechirped signal to obtain the frequency of interest, f_s .

Once we have the frequency, f_s , we can determine the range. The range to the target can be obtained from the following formula:

$$R = \frac{f_s c}{2k} \quad [2.5-3]$$

This relationship also forms the basis of the formula to be used to find the range resolution of our system. Range resolution is a parameter that gives the minimum range separation two targets can have and still be resolved as two distinct targets. It is dependent on the pulse length of our system, T . The range resolution, ΔR , can be obtained from the following formula:

$$\Delta R = \frac{c}{2kT} \quad [2.5-4]$$

This relationship is still bandwidth dependent since $kT = B = 1/\tau$. The term τ is the duration of the pulse after compression. The ΔR obtained for our system is the same as the one obtained from a short-pulse system of duration τ .

Pulse compression is used to obtain a signal processing gain and improve the SNR. The amount of compression gain obtained from the system is seen from the *pulse compression ratio*, which is simply the ratio of the transmitted pulse duration, T , to the system's effective pulse duration, τ and is given by:

$$CR = T/\tau \quad [2.5-5]$$

The effective pulse duration, $\tau = 1/B$, where B is the chirp bandwidth. For our system $B = 260$ MHz and $T = 40$ μ s, which gives a chirp rate of $k = 6.5$ MHz/ μ s. ΔR for our system is 0.576 m. These values give a compression gain of about 40 dB. When this gain is applied to the SNR of -38 dB obtained previously, the SNR increases to about 2 dB. At this point the SNR needs further improvement for detection.

2.6 Coherent Integration

When the modulated pulse is transmitted, it reaches the target and is backscattered. A portion of the backscattered signal reaches the receiver, is processed, and then digitized. This signal is a sinusoid, which is buried in noise. This process is repeated for each transmitted signal. The phase and frequency are the same for each pulse. The noise in the received signals, however, is random and is different for each pulse.

If the received sinusoids are added together, the sinusoid part will add constructively while the noise will add destructively, because noise is uncorrelated. As the received signals are averaged together, the signal power will stay the same while the noise power level will be reduced, yielding an improved SNR. The following expression gives the mathematical formula for this averaging called coherent integration.

$$\overline{S_{rx}(n)} = \frac{1}{N} \sum_n^N S_{rx}(n) \quad \text{for } n = 1, 2, \dots, N \quad [2.6-1]$$

where

N = number of signals averaged

The signal processing gain obtained from the averaging is N. So, if 10 coherent integrations are performed, the SNR will be improved by 10 dB. However, we should keep in mind that this process has its limits for improving SNR. This limit is due to non-random system noise dominating the noise term when the noise floor is reduced to a certain limit. Since this noise source is not random, the averaging does not reduce the noise floor and the SNR is not improved. Increasing the number of coherent integrations also increases the sampling area of the target. This is due to the fact that the satellite is moving and the target is stationary. For our case, we only need about 10 dB of SNR improvement for target detection, which is well within the limits of this process.

When the 10 dB improvement is added to the SNR of 2 dB obtained after pulse compression, we get an SNR of 12 dB.

We can make sure that an SNR of 12 dB is enough to get a range accuracy of 10 cm. We know from [2.2-1] that the range accuracy is:

$$\sigma_R = \frac{c}{2 B \sqrt{2 SNR}}$$

For a pulse bandwidth of 260 MHz and an SNR of 12 dB, this equation predicts a range accuracy of 10.3 cm, which meets the science requirement.

2.7 Conclusion

The goal of this project is to design a laser radar that will measure the range to a scattering target 600 km away with a 1 m diameter-receiving aperture and have a range accuracy of 10 cm. When the incoherent detection scheme was used, the SNR obtained was -132 dB, which is too low for accurate range measurement. To improve this SNR, we used coherent detection, which provided an improvement of 94 dB with a P_{lo} of 1 mW. To further improve the SNR of the system, the pulse compression technique is introduced. With this technique, a chirp rate of $k = 260 \text{ MHz}/40 \mu\text{s}$ provided a 40 dB SNR improvement. Finally, the system's data collection system is configured to perform 10 coherent integrations, which brought the system's SNR to about 12 dB.

With all these techniques, we can measure the range to a target at 600 km with a range accuracy of 10 cm with a peak transmit power of 10 mW.

CHAPTER 3

System Design

3.1 Introduction

This chapter presents the system design that would achieve the performance described in Chapter 2. It will be used as a prototype for the laser radar project. The explanation for choosing the system parameter values will be presented in Chapter 5.

3.2 System Block Diagram

In this section, the block diagram is presented to explain the system design. Figure 3.2-1 shows this block diagram that will be used to implement the concepts presented in Chapter 2. It has three main subsections: the transmitter, the receiver and the signal processing sections. The transmitting and receiving subsections have both optical and RF parts. The RF parts are shown in orange while the optical parts are shown in yellow in the figure. The digital components of the system such as data acquisition and timing and control are shown in blue.

In the next section, we will look at how the system works and present mathematical representations for signals produced at different sections of the system to better understand how everything works.

Hybrid RF/Laser Radar Block Diagram

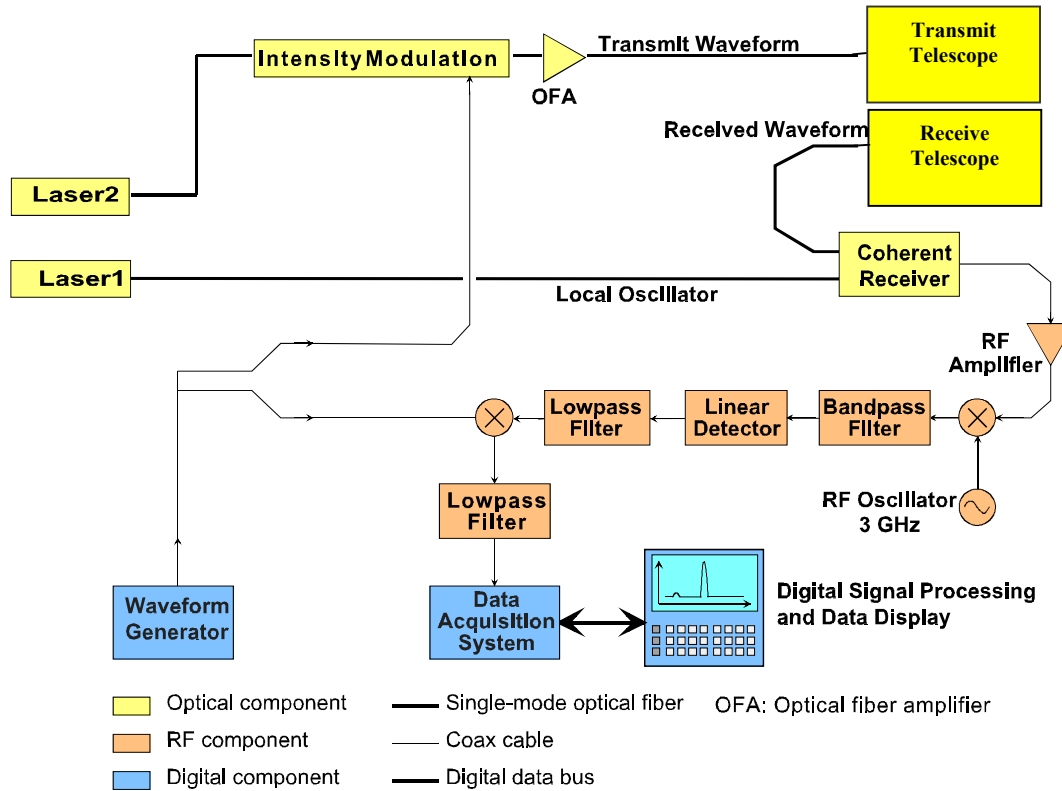


Figure 3.2-1: The hybrid RF/laser radar block diagram.

3.3 How the System Works

As seen from the block diagram, we have two optical signals shown to be outputs from laser1 and laser2. Laser2 outputs light that is intensity modulated to get the transmit signal. It is intensity modulated with a chirp signal, $m(t)$, produced by the waveform generator.

The expression for $m(t)$ is given below:

$$m(t) = a \cos(2 \pi f_C t + 0.5 k t^2 + \phi_C) \quad [3.3-1]$$

where

$m(t)$ = the chirp waveform [V]

f_C = the chirp start frequency [Hz]

k = the chirp rate [s^{-2}]

a = the modulation index of the chirp waveform ($0 < a \leq 1$)

ϕ_C = the chirp start phase [radians]

After the optical signal is intensity modulated, it is transmitted. This signal is labeled as $q(t)$ and is expressed as follows:

$$q(t) = \frac{A}{2} [1 + m(t)] \cos(2 \pi f_{TX} t + \phi_{TX}) \quad [3.3-2]$$

where

$q(t)$ = transmit signal [V]

A = amplitude of the transmitted signal [V]

f_{TX} = optical frequency of the transmit signal [Hz]

ϕ_{TX} = phase of the optical transmitted signal [radians]

This signal received from the target, $r(t)$, reaches the receiving aperture of the system and is captured. The expression for $r(t)$ (ignoring effects of frequency instability and Doppler) is as follows:

$$r(t) = \frac{A \alpha}{2} [1 + m(t - \tau)] \cos[2 \pi f_{TX} (t - \tau) + \phi_{RX}] \quad [3.3-3]$$

where

$r(t)$ = received signal [V]

α = round-trip loss factor ($0 < \alpha < 1$)

ϕ_{RX} = phase of the received signal [radians]

τ = round-trip signal travel time [s]

This signal then goes through the coherent detection process. As explained in Chapter 2, this process requires a local oscillator (LO) signal. This signal, $p(t)$, is supplied here by laser 1. The frequency of this signal differs from that of laser 2 by f_s . The expression for the LO signal is:

$$p(t) = \cos [2\pi(f_{TX} + f_s)t + \phi_{LO}] \quad [3.3-4]$$

where

$p(t)$ = local oscillator signal [V]

f_s = frequency shift of the LO signal [Hz]

ϕ_{LO} = starting phase of the LO signal [radians]

Figure 3.3-2 shows the signals mentioned up to this point in frequency domain and is presented below for better understanding of the system.

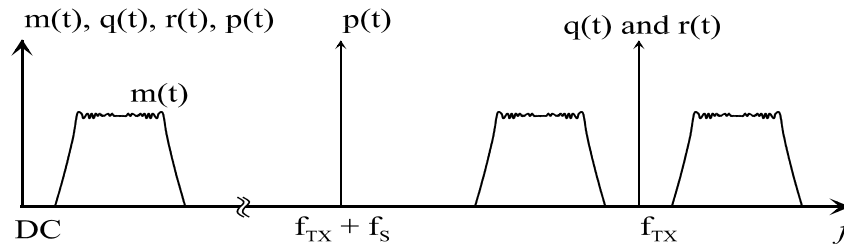


Figure3.3-2: Signals of interest in frequency domain.

During the detection process, thermal and shot noise with bandwidth B_R are introduced to the system. These are assumed to be the only noise sources in the system. This noise term is $n(t)$ and its expression is given below:

$$n(t) = n_o \{ \cos[\theta_n(t)] + j \sin[\theta_n(t)] \} \quad [3.3-5]$$

where

$n(t)$ = noise term [V]

$\theta_n(t)$ = random phase that follows a uniform distribution [radians]

The signal from the coherent receiver is $s(t) + n(t)$, where $s(t)$ denotes the result of square-law detection of the return signal $r(t)$ with the LO signal $p(t)$. The expression for $s(t)$ is given below:

$$s(t) = \Re [r(t) + p(t)]^2 \quad [3.3-6]$$

where

$s(t)$ = detected signal [V]

\Re = photodiode responsivity [A/W]

$$s(t) = \Re \left\{ \frac{A \alpha}{2} [1 + m(t - \tau)] \cos[2 \pi f_{TX} (t - \tau) + \phi_{RX}] + \cos [2 \pi (f_{TX} + f_s) t + \phi_{LO}] \right\}^2$$

$$s(t) = \Re \{ (A \alpha / 2)^2 [1 + m(t - \tau)]^2 \cos^2 [2 \pi f_{TX} (t - \tau) + \phi_{RX}] + \cos^2 [2 \pi (f_{TX} + f_s) t + \phi_{LO}] \\ + A \alpha [1 + m(t - \tau)] \cos[2 \pi f_{TX} (t - \tau) + \phi_{RX}] \cos[2 \pi (f_{TX} + f_s) t + \phi_{LO}] \}$$

$$s(t) = \frac{\Re}{2} \{ (A \alpha / 2)^2 [1 + 2 m(t - \tau) + m^2(t - \tau)] \{ 1 + \cos[2 \pi 2 f_{TX} (t - \tau) + 2 \phi_{RX}] \} \\ + \{ 1 + \cos[2 \pi 2 (f_{TX} + f_s) t + 2 \phi_{LO}] \} \\ + A \alpha [1 + m(t - \tau)] \{ \cos(-2 \pi f_s t - 2 \pi f_{TX} \tau + \phi_{RX} - \phi_{LO}) \\ + \cos[2 \pi f_{TX} (t - \tau) + \phi_{RX} + 2 \pi (f_{TX} + f_s) t + \phi_{LO}] \} \\ + \cos[2 \pi f_{TX} (2 t - \tau) + \phi_{RX} + \phi_I] \} \\ + \cos[2 \pi (2 f_{TX} + f_s) t + \phi_{LO} + \phi_I] \}$$

Since optical signals and harmonics of optical signals are suppressed, this expression reduces to:

$$s(t) = \frac{\Re}{2} \{ [A \alpha / 2]^2 [1 + 2 m(t - \tau) + m^2(t - \tau)] + 1 + A \alpha [1 + m(t - \tau)] \cos(-2 \pi f_s t - 2 \pi f_{TX} \tau + \phi_{RX} - \phi_{LO}) \}$$

To obtain the total coherent receiver output, the noise term $n(t)$ should be added as shown below:

$$s(t) + n(t) = \frac{\Re}{2} \{ [A \alpha / 2]^2 [1 + 2 m(t - \tau) + m^2(t - \tau)] + 1 \\ + A \alpha [1 + m(t - \tau)] \cos(-2 \pi f_s t - 2 \pi f_{TX} \tau + \phi_{RX} - \phi_{LO}) \} + n(t) \quad [3.3-7]$$

This signal is then passed through a bandpass filter of bandwidth B_1 . This filter rejects the DC and double frequency terms together with the baseband chirp and chirp-squared terms, and the following expression is obtained:

$$u(t) = \frac{\Re A \alpha}{2} [1 + m(t - \tau)] \cos(-2 \pi f_s t - 2 \pi f_{TX} \tau + \phi_{RX} - \phi_{LO}) + n(t) \frac{B_1}{B_R} \quad [3.3-8]$$

where

$u(t)$ = output of the first bandpass filter [V]

B_1 = bandwidth of the first bandpass filter [Hz]

B_R = receiver bandwidth [Hz]

The following figure shows the baseband chirp and chirp-squared terms, which are rejected by the bandpass filter, in addition to the terms inside the passband.

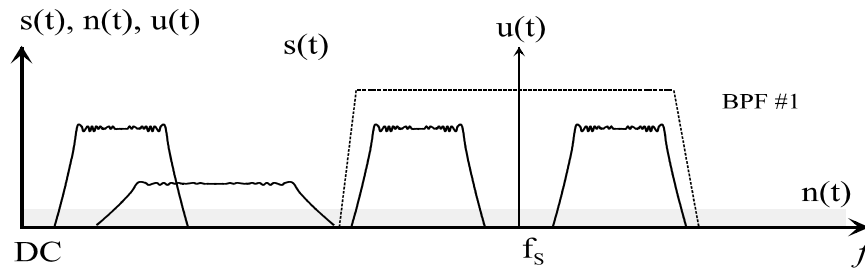


Figure 3.3-3 The various signals in the system.

The output of the bandpass filter is then fed to the linear detector to obtain the signal of interest from the envelope of $u(t)$. The output of this square-law detection process is $v(t)$ and the expression of $v(t)$ is given below:

$$v(t) = \eta [u(t)]^2 \quad [3.3-9]$$

$$v(t) = \eta \left\{ \frac{\Re A \alpha}{2} [1 + m(t - \tau)] \cos(-2 \pi f_s t - 2 \pi f_{TX} \tau + \phi_{RX} - \phi_{LO}) + n(t) \frac{B_1}{B_R} \right\}^2$$

$$\begin{aligned}
v(t) &= \eta \left\{ \frac{\Re A \alpha}{2} [1 + m(t - \tau)] \cos(2 \pi f_s t - 2 \pi f_{TX} \tau + \phi_{RX} - \phi_{LO}) \right\}^2 \\
&\quad + \eta \Re A \alpha [1 + m(t - \tau)] \cos(2 \pi f_s t - 2 \pi f_{TX} \tau + \phi_{RX} - \phi_{LO}) n(t) \frac{B_1}{B_R} + \eta n^2(t) \left(\frac{B_1}{B_R} \right)^2 \\
v(t) &= \eta \left(\frac{\Re A \alpha}{2} \right)^2 [1 + m(t - \tau)]^2 \cos^2(2 \pi f_s t - 2 \pi f_{TX} \tau + \phi_{RX} - \phi_{LO}) \\
&\quad + \eta \Re A \alpha [1 + m(t - \tau)] \cos(2 \pi f_s t - 2 \pi f_{TX} \tau + \phi_{RX} - \phi_{LO}) n(t) \frac{B_1}{B_R} + \eta n^2(t) \left(\frac{B_1}{B_R} \right)^2
\end{aligned}$$

where

$v(t)$ = output of the linear detector [V]

η = detector efficiency ($0 < \eta < 1$)

The output of the linear detector is then passed through a second bandpass filter to reject DC, double-chirp, and IF terms. The expression for its output is given below:

$$w(t) = \eta \left(\frac{\Re A \alpha}{2} \right)^2 m(t - \tau) + \eta \Re A \alpha n(t) \frac{B_1}{B_R} + \eta n^2(t) \left(\frac{B_1}{B_R} \right)^2 \quad [3.3-10]$$

where

$w(t)$ = output of the second bandpass filter [V]

The signal $w(t)$ is then mixed with the original chirp signal to obtain the dechirped signal $x(t)$. Its expression is shown below:

$$x(t) = m(t) \left[\eta \left(\frac{\Re A \alpha}{2} \right)^2 m(t - \tau) + \eta \Re A \alpha n(t) \frac{B_1}{B_R} + \eta n^2(t) \left(\frac{B_1}{B_R} \right)^2 \right] \quad [3.3-11]$$

where

$x(t)$ = dechirped signal [V]

To better understand how the signal that is input to the signal processor, $y(t)$, is obtained, the following analysis of dechirping is presented. It shows the original chirp signal, $m(t)$, mixed with the chirp signal that has a time delay, τ , due to its travel time to the target.

$$m(t) m(t - \tau) = a \cos(2 \pi f_c t + 0.5 k t^2 + \phi_c) a \cos[2 \pi f_c (t - \tau) + 0.5 k (t - \tau)^2 + \phi_c] \quad [3.3-12]$$

$$m(t) m(t - \tau) = \frac{a^2}{2} [\cos(2 \pi f_c \tau + k t \tau - 0.5 k \tau^2) + \cos(2 \pi 2 f_c t - 2 \pi f_c \tau + k t^2 - k \tau t + 0.5 k \tau^2 + 2 \phi_c)]$$

Of the terms seen above, the cosine term with $2 \pi f_c \tau$ has the target range information. When this product is low-pass filtered, the following expression is obtained, which contains the signal of interest:

$$y(t) = \frac{\eta(\Re A \alpha a)^2}{8} \cos(2 \pi f_c \tau + k t \tau - 0.5 k \tau^2) + \eta \Re A \alpha m(t) n(t) \left(\frac{B_1}{B_R} \right) + \eta n^2(t) \left(\frac{B_1}{B_R} \right)^2 m(t) \quad [3.3-13]$$

where

$$y(t) = \text{signal to be signal processed [V]}$$

When $y(t)$ is obtained, it is input to the signal processor. The signal processor performs the FFT to obtain the frequency domain representation of the signal. When the spectrum of the signal is at hand, all the parts except for the part containing the signal is filtered out. This is done to reject noise and any other undesired signals. The following section explains the processes in the signal processing section.

3.4 Signal Processing

During the signal processing section of the detection process, the spectrum of the signal is obtained by performing an FFT on $y(t)$. The length of the FFT is fixed since the signal has fixed pulsewidth. This limited pulsewidth restricts the time to collect data and take FFT. Hence, the binwidth of the FFT is fixed.

Once the FFT is performed, the unwanted parts of the incoming signal are filtered out to obtain the signal of interest. Coherent integrations are performed to improve the SNR. The premise behind coherent integration is explained in Chapter 2 in detail, but the general idea is to improve SNR by reducing random noise level. Since the signal of interest is not random, this process does not affect it.

The expression SNR per bin is shown below. This is easily obtained since noise and signal per bin are known and SNR per bin is found by taking the ratio of signal per bin to noise per bin.

$$\text{SNR per bin} = \frac{\frac{\eta (\mathfrak{R} A \alpha a)^2}{8} \cos(2 \pi f_c \tau + k t \tau - 0.5 k \tau^2)}{\eta \mathfrak{R} A \alpha m(t) n(t) \left(\frac{B_i}{B_r} \right) + \eta n^2(t) \left(\frac{B_i}{B_r} \right)^2 m(t)} \quad [3.4-1]$$

The numerator represents the signal while the denominator represents the noise. The first term in the denominator contains the $n(t)$ term, which has a Gaussian distribution and is reduced.

Once the signal is easily observed in the spectrum, its frequency is obtained. This frequency information is then used to obtain the range to the target using the following formula:

$$\text{Range to target} = \frac{(\text{signal frequency})(\text{speed of light})}{(\text{chirp rate})} \quad [3.4-2]$$

While this expression provides the range information, the range accuracy can be obtained from the SNR information using [2.2-1].

CHAPTER 4

Simulations

4.1 Introduction

The following chapter presents simulations done with Matlab to predict the behavior of the laser radar system under different conditions with different parameters. Simulations are carried out so that system performance can be predicted without the need to make changes in hardware. The program code used is given in Appendix A. (It is important to note that the program presented in this appendix is one copy of the program that is modified for each task to get results. In other words, if the effects of parameter A are to be observed, the program is modified to take this parameter as a variable user input. Then another variable is given as a variable in the same manner to observe its effects.)

First presented is a block diagram containing each step of the simulation to help the reader understand the simulation process better. Also presented are the values of the parameters used and their variable names used in the program.

Next is the presentation of simulation results obtained by changing selected parameters and seeing their effect on target detection. To help explain the results better they are given in a table or graph or both. Some of the plots provided have a fitted line with the actual data to see the relationship between the parameters more clearly. The equation for the fitted line is given in the plots.

4.2 System Parameters and Block Diagram

In this section a block diagram is presented and each step of the simulation is explained. This explanation also includes time- or frequency-domain plots for some of the signals to provide visual information to the reader. Also presented are the values of the parameters used and their variable names used in the program.

Figure 4.2-1 below shows the block diagram that gives a visual representation of the simulation program used.

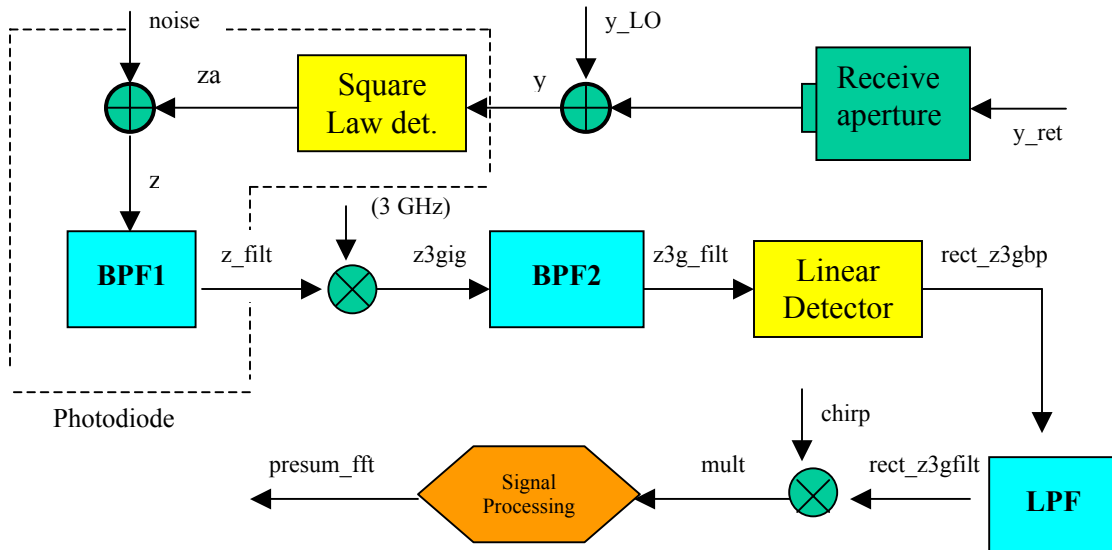


Figure 4.2-1 Simulation system diagram.

As seen from this figure, the simulation focuses on the receiver. This is due to the need to maximize the receiver sensitivity for the detection of the weakest signal possible.

To obtain meaningful results that predict our system behavior, most of the parameters used are same as the ones in the actual system, while a few are different to provide faster operation of the simulation. (One of these parameters is the carrier frequency. The simulation uses a value of 2 GHz instead of the actual THz range carrier.) Given below are the values of the parameters and the variable names (in *italics*) used in the simulation program.

Modulation index [mi] = 0.9
 Responsivity [$Resp$] = 1 A/W
 Local oscillator power [Pwr_lo] = 0.5 mW
 Pulse duration [$pulsewidth$] = 10 us
 Receiver bandwidth [BW_rec] = 2.5 GHz
 Carrier frequency [w_car] = $2 \cdot \pi \cdot 2 \times 10^9$ radians/s
 Local oscillator frequency [w_lo] = $2 \cdot \pi \cdot 2.6 \times 10^9$ radians/s
 Chirp bandwidth [$bandwidth$] = 260 MHz
 Chirp start frequency [w] = 200 MHz
 NEP (noise equivalent power) [NEP] = 24 pA/ $\sqrt{\text{Hz}}$

The transmitted signal is scattered from the target and a portion reaches the receiving aperture. This signal is labeled **y_ret** in the simulation and is mixed with the local oscillator signal (**y_LO**) to simulate the coherent detection process. (The frequency-domain representations on these signals are given in Figures 4.2-2 and 4.2-3, respectively.) For the scattered signal, the chirp-modulated signal is seen with the carrier at 2 GHz. The similar signal occurring at 8 GHz is the image signal and is not real.

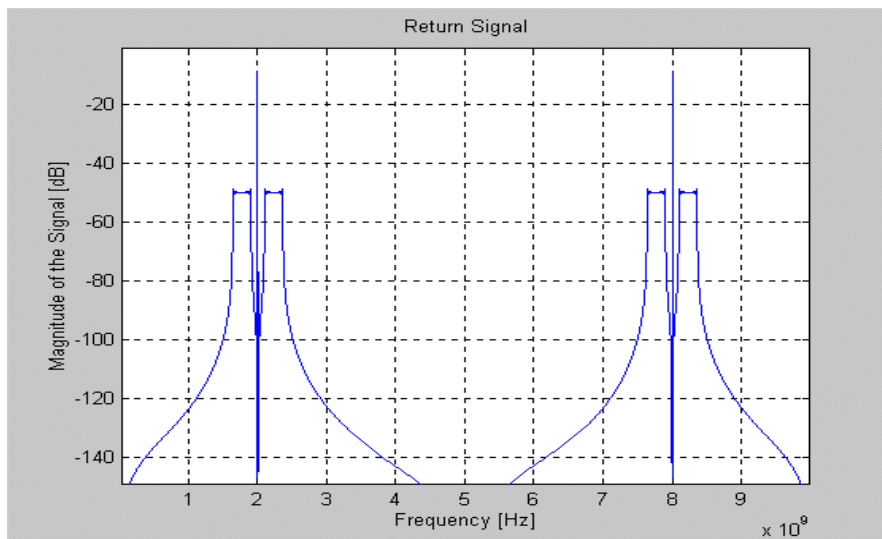


Figure 4.2-2: The scattered signal in frequency domain [**y_ret**].

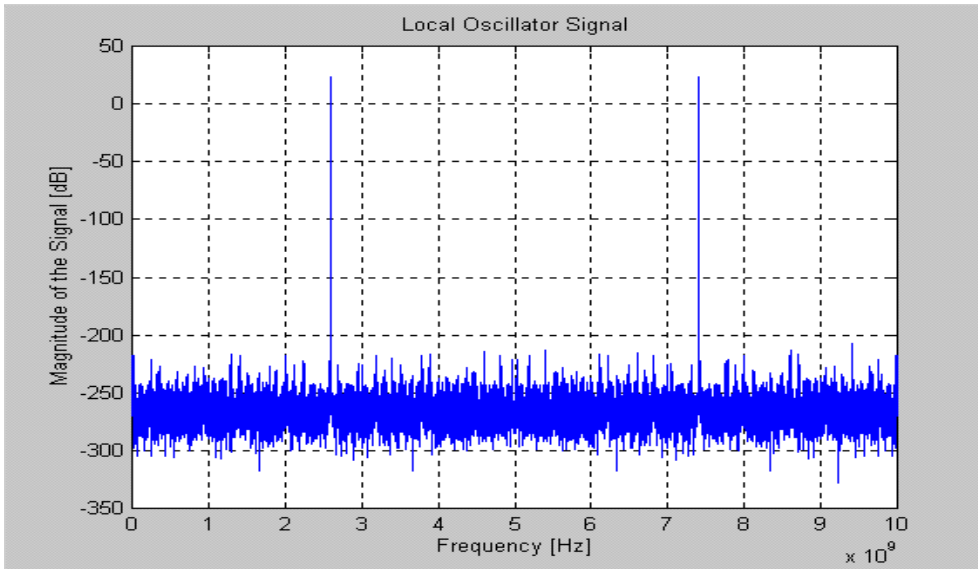


Figure 4.2-3: The local oscillator signal in frequency domain [y_LO].

The output of this mixer, y , is input to the photodiode for detection. The detection process is modeled as square-law detection and the output of the square-law detector, z_a , is shown in Figure 4.2-4 below.

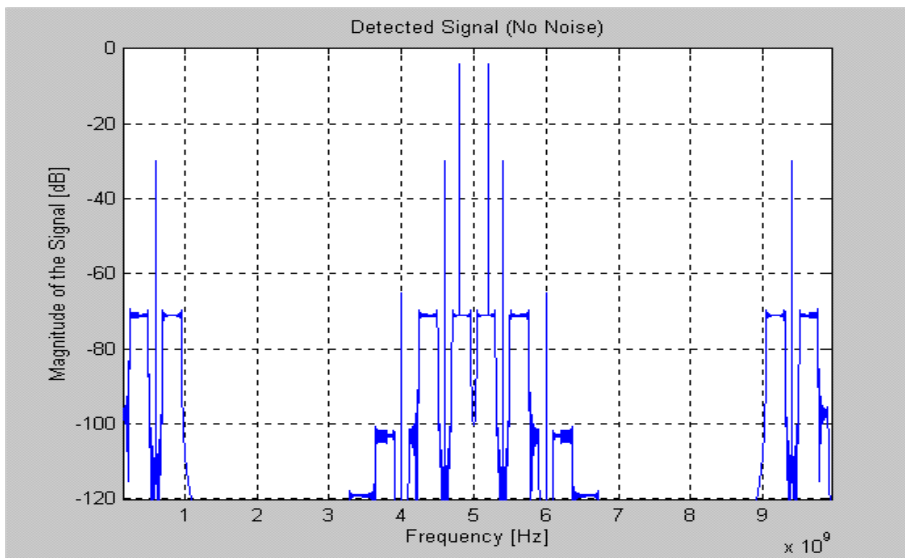


Figure 4.2-4: The detected signal (no noise) in frequency domain [z_a].

A Gaussian noise vector, **noise**, is created and added to the detected signal to simulate the noise introduced in the photo diode. As seen in Appendix A, this noise vector in the

simulation is obtained by creating thermal and shot noise vectors and adding them to get the **noise** vector. The detected signal with noise is, **z**, is shown in Figure 4.2-5.

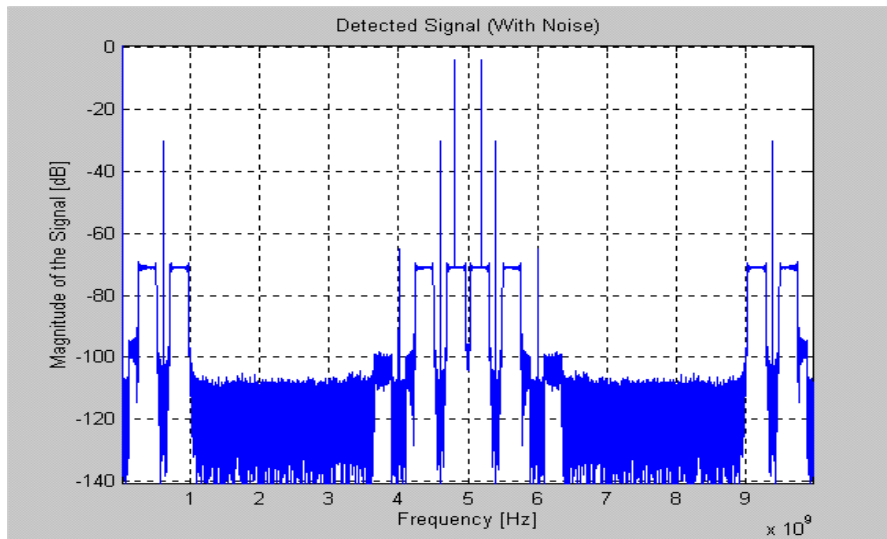


Figure 4.2-5: The detected signal (with noise) in frequency domain [z].

This signal is filtered by the first bandpass filter with its lower cutoff frequency at 160 MHz and higher cutoff frequency at 1.06 GHz. This signal, **z_filt** (shown in Figure 4-2.6) is then multiplied by a 3 GHz signal to perform the frequency upconversion required by the linear detector. (This requirement will be discussed in Chapter 5.)

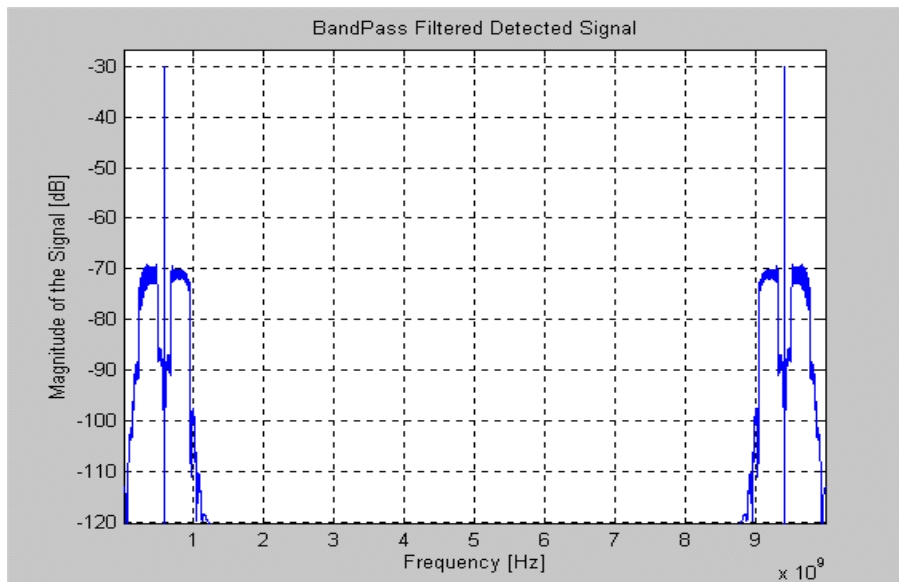


Figure 4.2-6: Bandpass filtered detected signal in frequency domain [z_filt].

The output of this multiplication is signal, **z3gig**, which is bandpass filtered before being sent to the envelope detector. This second bandpass filter has a passband from 3.2 GHz to 4 GHz. (The **z3gig** signal and the filtered signal **z3g_filt** are shown in Figures 4.2-7 and 4.2-8, respectively.)

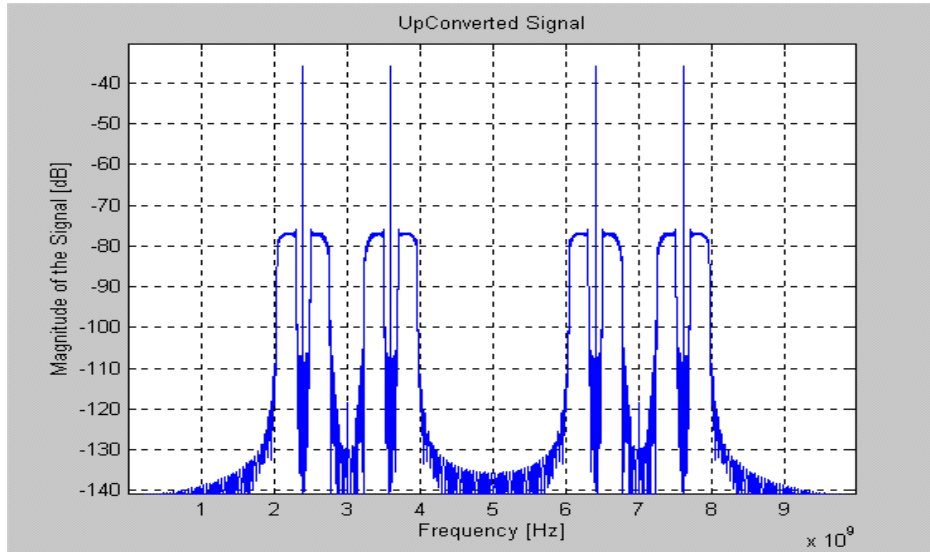


Figure 4.2-7: The upconverted signal in frequency domain [z3gig].

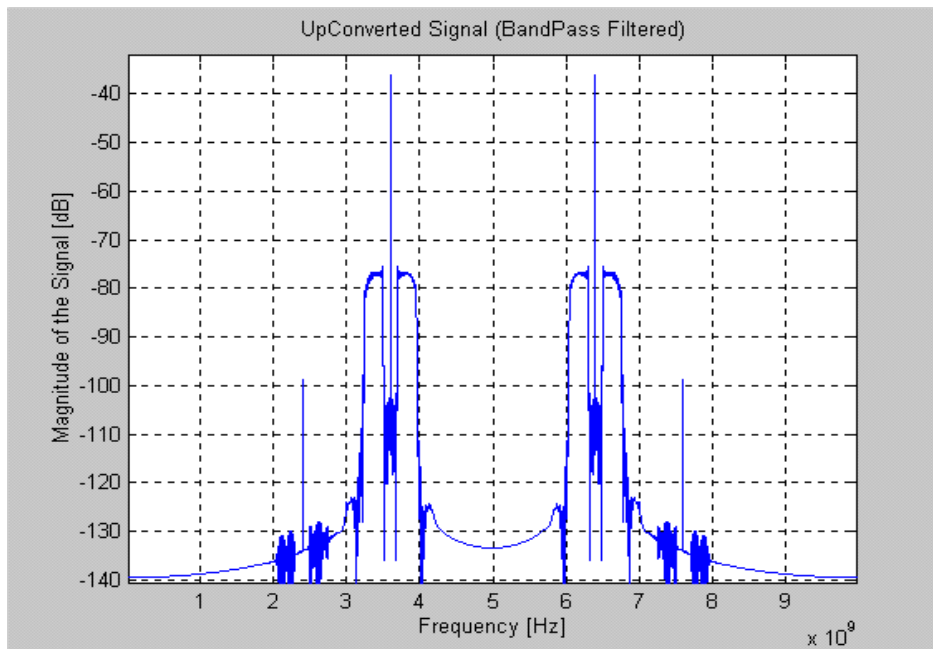


Figure 4.2-8: The upconverted signal (bandpass filtered) in freq. domain [z3g_filt].

The filtered signal, **z3g_filt**, is input to the module in the program that simulates linear detection (rectification) and the output signal is **rect_z3gbp**. Figures 4.2-9 and 4.2-10 show the input and output signals to the linear detector in time domain.

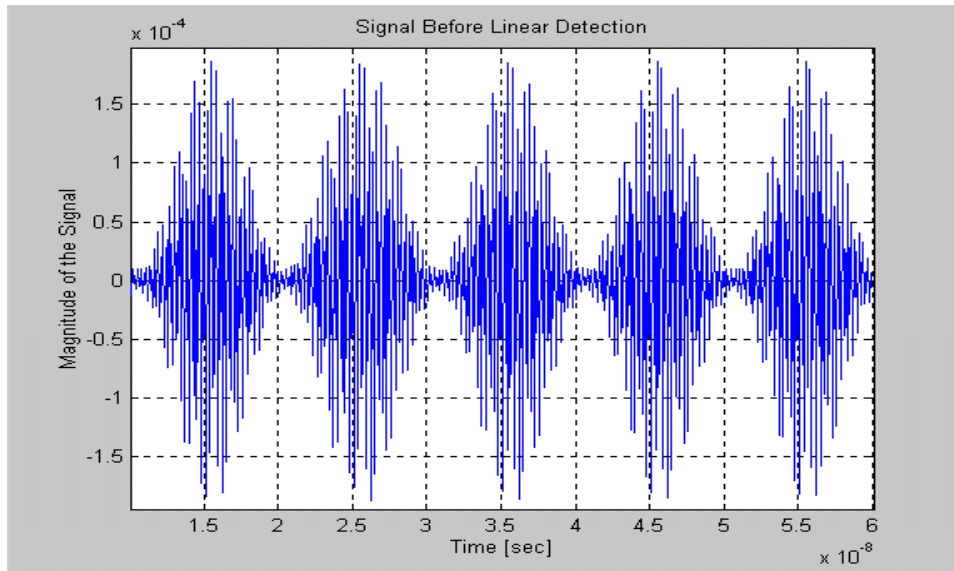


Figure 4.2-9: The signal input to the linear detector in time domain [z3g_filt].

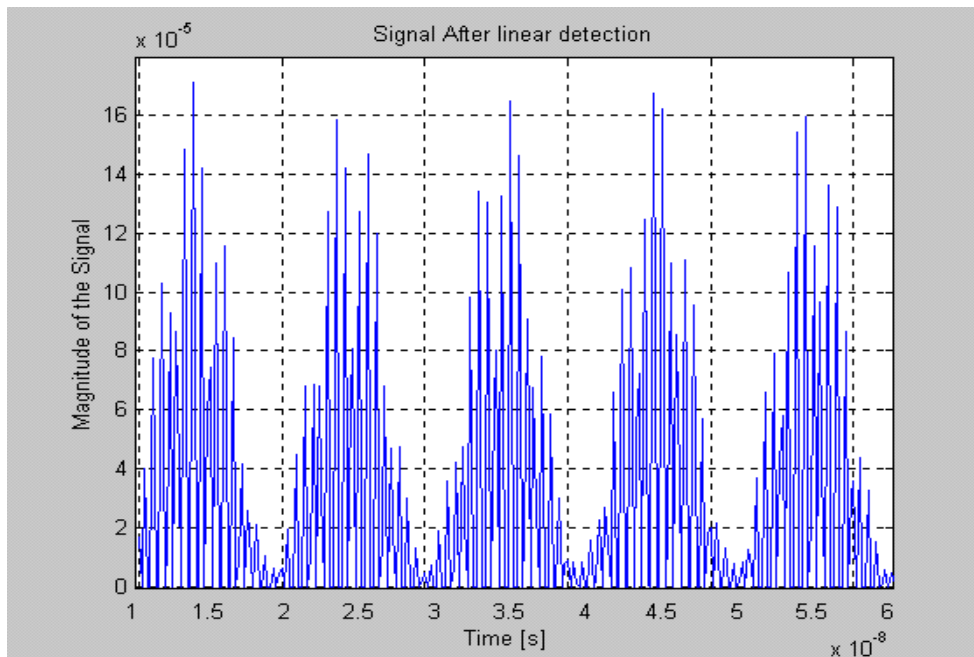


Figure 4.2-10: The output signal of the linear detector in time domain [rect_z3gbp].

It is then lowpass filtered and centered at zero before the dechirping process. Figures 4.2-11 and 4.2-12 show the output of this low-pass filter in both time and frequency domain.

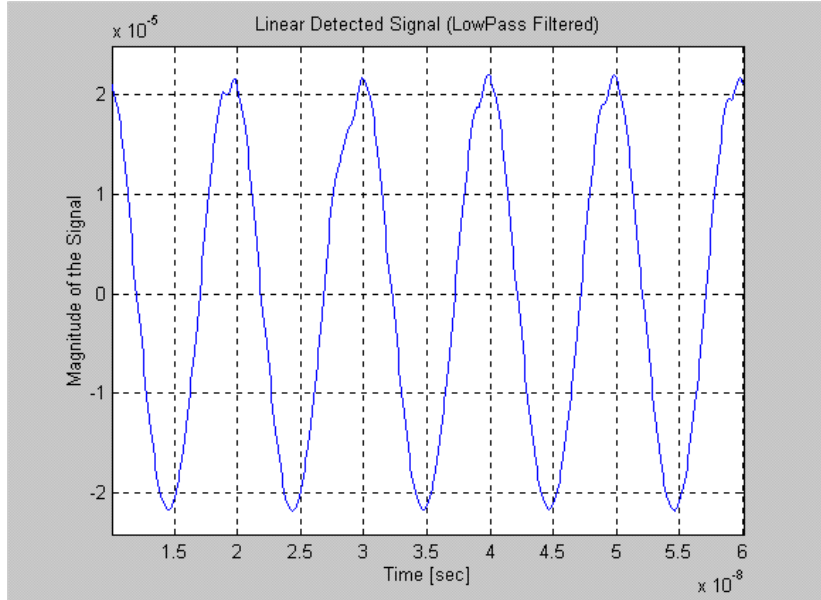


Figure 4.2-11: Linear detected signal (LP filtered) in time domain [rect_z3gfilt].

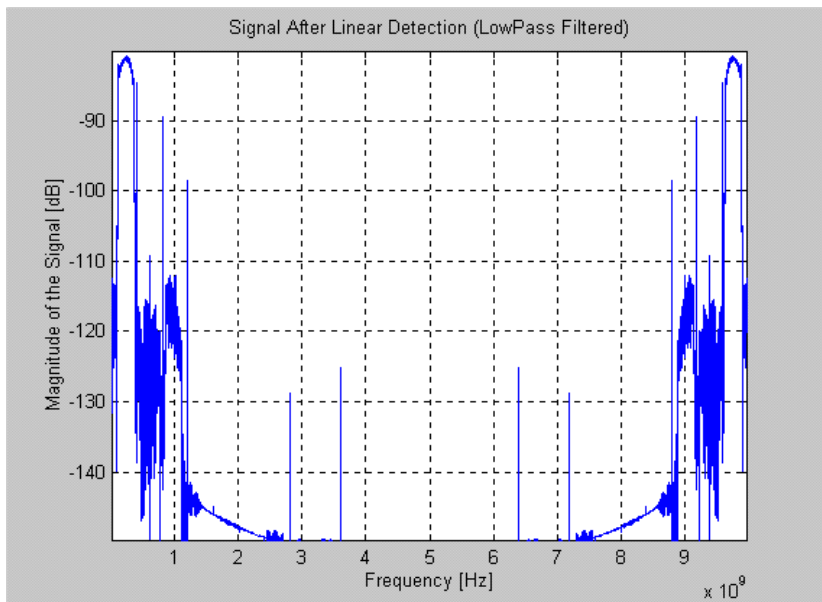


Figure 4.2-12: Linear detected signal (LP filtered) in freq. domain [rect_z3gfilt].

The output of the lowpass filter (**rect_z3gfilt**) is multiplied with the original chirp signal (**chirp**) to obtain the dechirped signal, **mult**. Figures 4.2-13 and 4.2-14 show this dechirped signal in time and frequency domains, respectively.

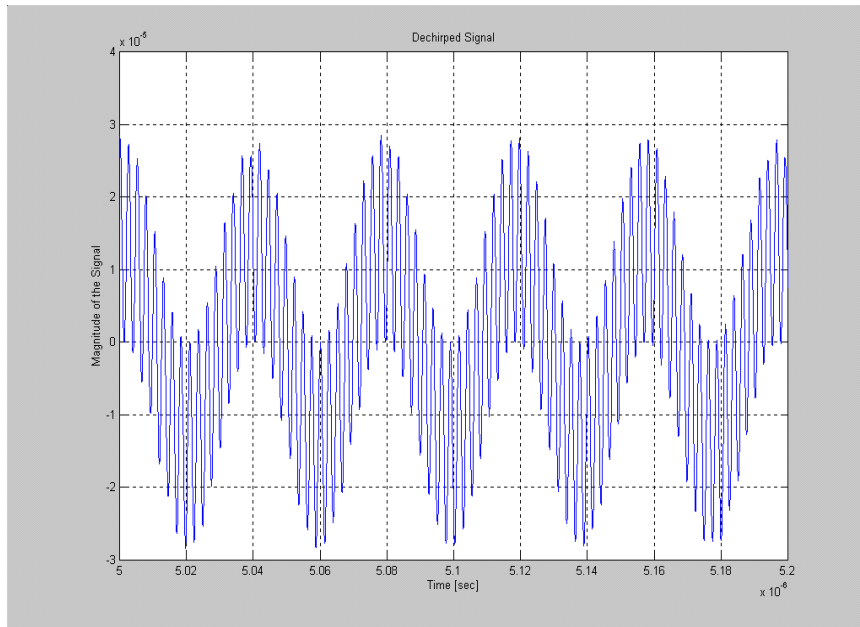


Figure 4.2-13: The dechirped signal in time domain [mult].

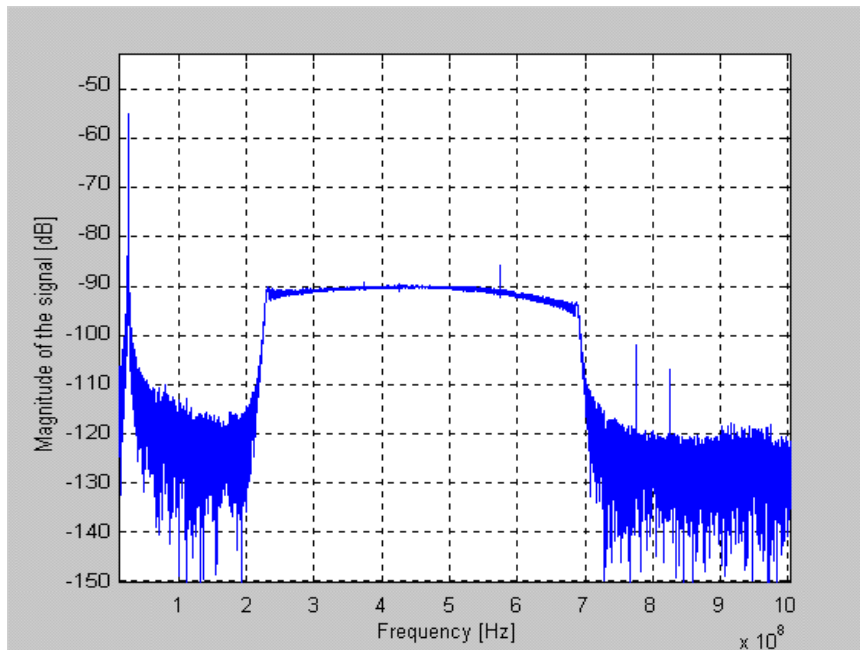


Figure 4.2-14: The dechirped signal in freq. domain [mult].

This signal is then sent to the signal-processing module to obtain the frequency domain representation of the **presum_fft** signal. If this signal is weak, the effects of signal processing methods like coherent integrations can be seen on this final result. Figure 4.2-15 shows the part of this signal spectrum that contains the frequency information for the target.

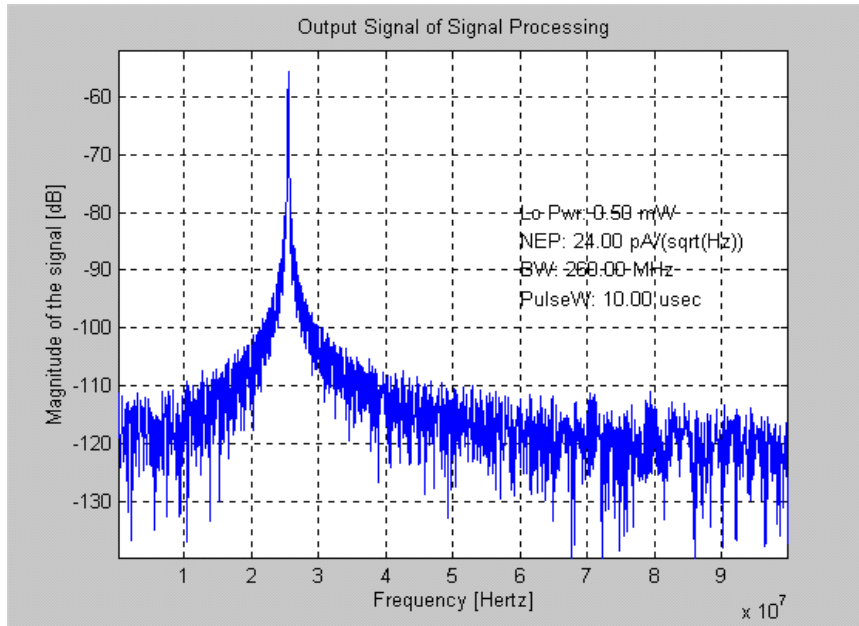


Figure 4.2-15: The output of the signal processor in freq. domain [**presum_fft**].

4.3 The Effects of Coherent Integrations on the Output SNR of the System

One of the important operations to be used in our system to improve system performance is coherent integration. In the most basic sense, coherent integrations average collected data to reduce the noise effects on the final result. This operation helps reduce noise since noise is random for the given segment while the signal is repetitive.

The Matlab program used is modified to ask the user the number of coherent integrations performed. The number of coherent integrations is increased by an

increment of 10. Then the signal and noise powers and the signal-to-noise ratio are determined. Here are the results obtained from the simulation.

Table 4.3-1: The simulation results for testing the effects of coherent integrations on SNR.

Input Optical Pwr[dBm]	No coh int	Signal Power[dB]	Noise Power[dB]	SNR out [dB]
-93.01	1	-125.28	-141.13	15.85
-93.01	10	-125.28	-150.9	25.62
-93.01	100	-125.38	-160.18	34.8

In this table, the first column denotes the optical power as received by the receiving aperture of the laser radar system. The second column shows how many times the received signal is averaged, while columns three through five show the signal power, noise power, and signal-to-noise ratio at the output of the receiver, respectively.

These results suggest that a factor-10 increase in the number of coherent integrations increases the SNR at the output by 10 dB. This is obtained by the reduction of the noise level by 10 dB while the signal power stays the same. However, at some point the noise floor level cannot be reduced any lower since the quantization noise (which cannot be reduced by coherent integration) dominates.

4.4 The Effects of Varying Modulation Index on the Minimum Detectable Optical Input Power for the System

One of the parameters that enters into the equation for the modulated signal is the modulation index. Choosing the optimum value for the modulated signal is key since we would like to pack as much energy as possible into the transmitted pulse. As the transmitted signal's sidebands have more power, the minimum detectable signal power is lower assuming that the attenuation through the path the signal travels stays constant.

To see how changing the values for the modulation index affects the minimum detectable optical input power, P_{inopt_min} , the values for the modulation index are changed from 0.3 to 1. Then, for each case, the signal at the receiver is observed to see at which lowest input power level the output signal is still visible. This level is then labeled as the minimum detectable optical input power for that particular case. The results are presented in Table 4.4-1 and Figure 4.4-1 below.

Table 4.4-1: Results of observing effects of changing modulation index on minimum detectable optical input power

Modulation index, u	Minimum detectable optical input power, P_{inopt_min} [pW]
0.3	0.65
0.45	0.5
0.6	0.35
0.75	0.25
0.9	0.25
1	0.25

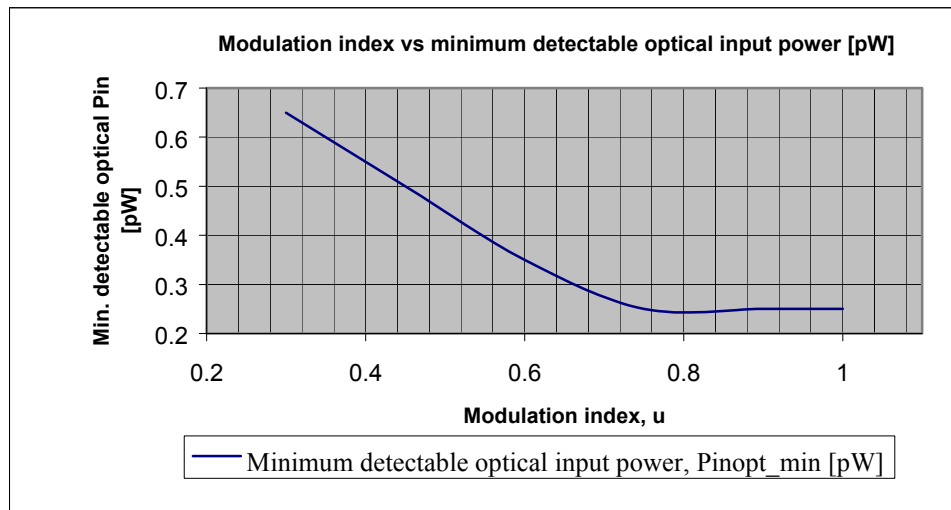


Figure 4.4-1: Modulation index vs. minimum detectable optical input power.

When we observe the table and figure above, we see that as the value of the modulation index is increased from 0.3 to 1, the minimum detectable optical input power decreases. In other words, when we use higher values of modulation index, we can detect

weaker signals, which is desired. However, it is seen from the plot above that this effect saturates around 0.8 and further increase of the modulation index does not improve the performance of the system. In accordance with the results of this simulation the modulation index for our system is chosen to be 1.

4.5 The Effects of Varying Noise Equivalent Power, NEP, on the Minimum Detectable Optical Input Power for the System

Another parameter that affects the performance of the laser radar system is the photodiode's noise equivalent power, NEP. It is used to describe the noise performance of a photodetector. For a given value of thermal noise, the photodetector will have an optical power value that will cause the signal-to-noise ratio, SNR, to be equal to 1 at its output. This level of optical power is referred to as the noise equivalent power, NEP. One important point to make is that values of receiver bandwidth and operating temperature should be specified to make the value of the NEP meaningful for each detector.

To see how changing the values for the NEP affects the minimum detectable optical input power, P_{inopt_min} , it is modified and the values for the NEP are changed from 2.4 pA/ $\sqrt{\text{Hz}}$ to 240 pA/ $\sqrt{\text{Hz}}$. Then, for each case, the signal at the receiver output is observed to see at which lowest input power level the output signal is still detectable. This level is then labeled as the minimum detectable optical input power for that particular case. The results are presented in Table 4.5-1 and Figure 4.5-1 below.

Table 4.5-1: The effects of NEP on minimum detectable optical input power.

NEP [pA/sqrt[Hz]	Minimum detectable optical input power, P_{inopt_min} [pW]
2.4	0.003
1.2	0.12
24	.2
120	11
240	20

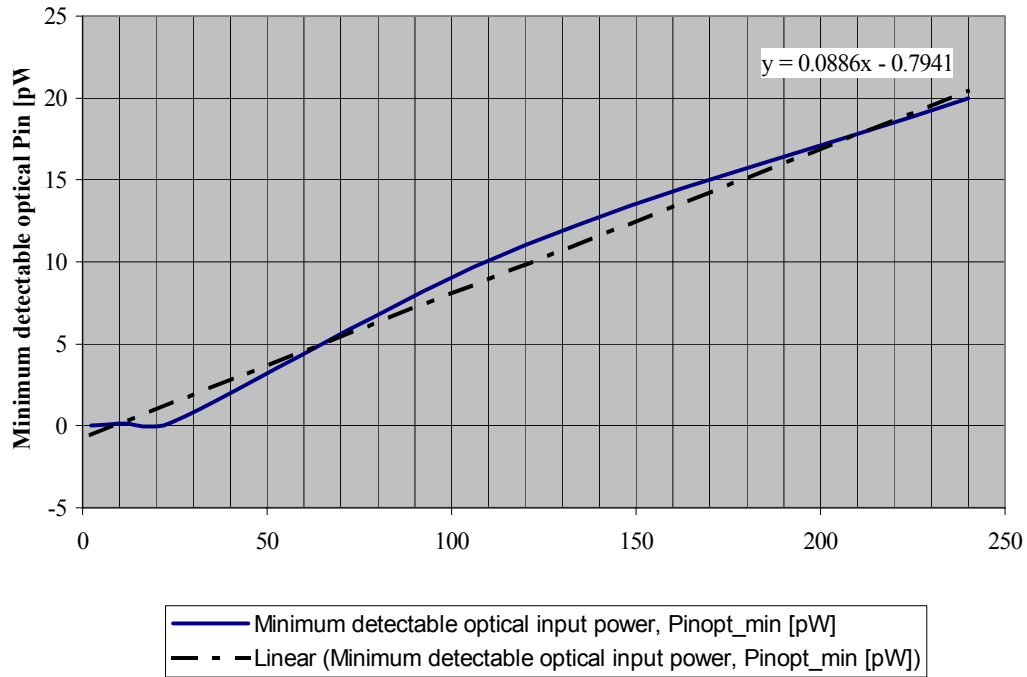


Figure 4.5-1: NEP vs. minimum detectable optical input power.

In addition to showing the relationship of NEP versus minimum detectable optical input power (the solid line), Figure 4.5-1 shows a fitted line, which approximates this relationship in the closest linear fashion (the dashed line). This is done to provide an additional tool for observing the relationship between the two parameters.

When the results are observed, it is seen that when the NEP is smaller, the system can detect weaker signals. This is expected since a smaller NEP means less noise in the photodetector giving way to weaker signals to be detected. In the end, the photodetector with the smallest NEP is chosen for the laser radar system.

4.6 The Effects of Varying Local Oscillator Power, P_lo, on the Minimum Detectable Optical Input Power for the System

The local oscillator power plays an important role in determining the minimum detectable optical input power for the system. This is because it mixes with the incoming optical signal before the square-law detection process. At the output of the detector the signal to be further analyzed is the cross term that is affected by the incoming signal power and the local oscillator power. A better way to see this term is to look at the mathematical model for the square-law detection:

$$(P_{\text{input_opt}} + P_{\text{LO}})^2 = P_{\text{input_opt}}^2 + P_{\text{LO}}^2 + 2 \mathbf{(P_{\text{input_opt}} P_{\text{LO}})} \quad [4.6-1]$$

where

$P_{\text{input_opt}}$ = input optical power

P_{LO} = local oscillator power

The term in bold in [4.6-1] is the cross term of the input signal power and the local oscillator power, and it is the term analyzed in the receiver to get target information needed. As this term clearly shows, the local oscillator power plays an important role for obtaining target information.

To see how changing the values for the local oscillator power affects the minimum detectable optical input power, the values for the local oscillator power are changed from 0.05 mW to 5 mW. Then, for each case, the signal at the receiver output is observed to see at which lowest input power level the output signal is still visible. This level is then chosen as the minimum detectable optical input power for that particular case. The results are presented in Table 4.6-1 and Figure 4.6-1.

Table 4.6-1: The effect of changing the local oscillator power on minimum detectable input power.

Local Oscillator Power (P_LO) [mW]	Minimum Detectable Input Optical Power [pW]
0.05	2.00
0.50	0.20
5.00	0.02

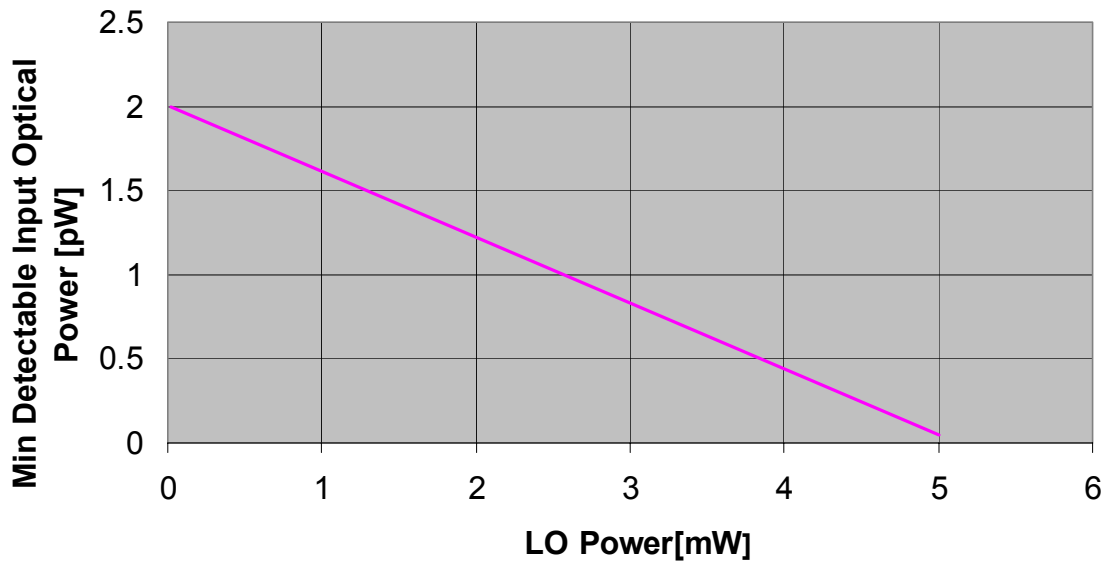


Figure 4.6-1: LO power versus minimum detectable input optical power.

As seen from the results presented, the lower the value for the local oscillator power, the stronger the incoming signal needs to be to be detected. In other words, to be able to detect weaker signals, the local oscillator power needs to be kept at its highest value.

4.7 Conclusion

In this chapter, the results of simulations were presented. These results were obtained from a program that simulates the operation of the laser radar system. They were helpful in predicting the system's behavior under different operating conditions without carrying out actual experiments.

One of the simulations predicted the effect of coherent integrations on the output SNR of the system. Since improving the SNR is essential for detecting weak return signals, it is important to know the relationship between coherent integrations and the output SNR. The simulation shows a one-to-one relationship between these parameters.

Another system parameter is the modulation index; its optimum value is predicted with the simulation results. The results show that the higher its value is to the maximum (which is 1), the better. This is determined by finding the minimum detectable optical input power possible for different values of modulation index.

The NEP's effect on the minimum detectable optical input power is observed. When the value of NEP is varied, we see that when the NEP is smaller, the system can detect weaker signals.

Finally, an optimum value for the local-oscillator signal power is predicted by observing the effects of its change on the minimum detectable input power. As expected, the higher the value for the LO power, the better weak signals are detected. Hence, the LO power value is to be chosen as high as possible within the system's capabilities.

In this chapter, a simulation tool used to predict system performance is presented. Certain parameters are changed to see their effects on the system. Next in Chapter 5, the simulation predictions are tested with the real system and its performance is observed.

CHAPTER 5

System Prototype and Experiment Results

5.1 Introduction

In this section, the system prototype built based on the theoretical analysis is presented. A system block diagram is presented and each of its components is discussed. Finally the results of experiments carried out with this prototype are presented. These experiments were carried out to test system performance and verify results predicted by calculations and simulations.

5.2 System Block Diagram

In Figure 5.2-1, the block diagram of the system prototype illustrates how the system works. It has three main subsections: the transmitter, the receiver, and the signal processor. The transmitting and receiving subsections have optical and RF parts. The RF parts are shown in orange while the optical parts are shown in yellow. The digital components of the system (e.g., data acquisition, timing and control) are shown in blue. The connections between optical parts are made by single-mode optical fibers while the connection for the RF sections are made with coaxial cables.

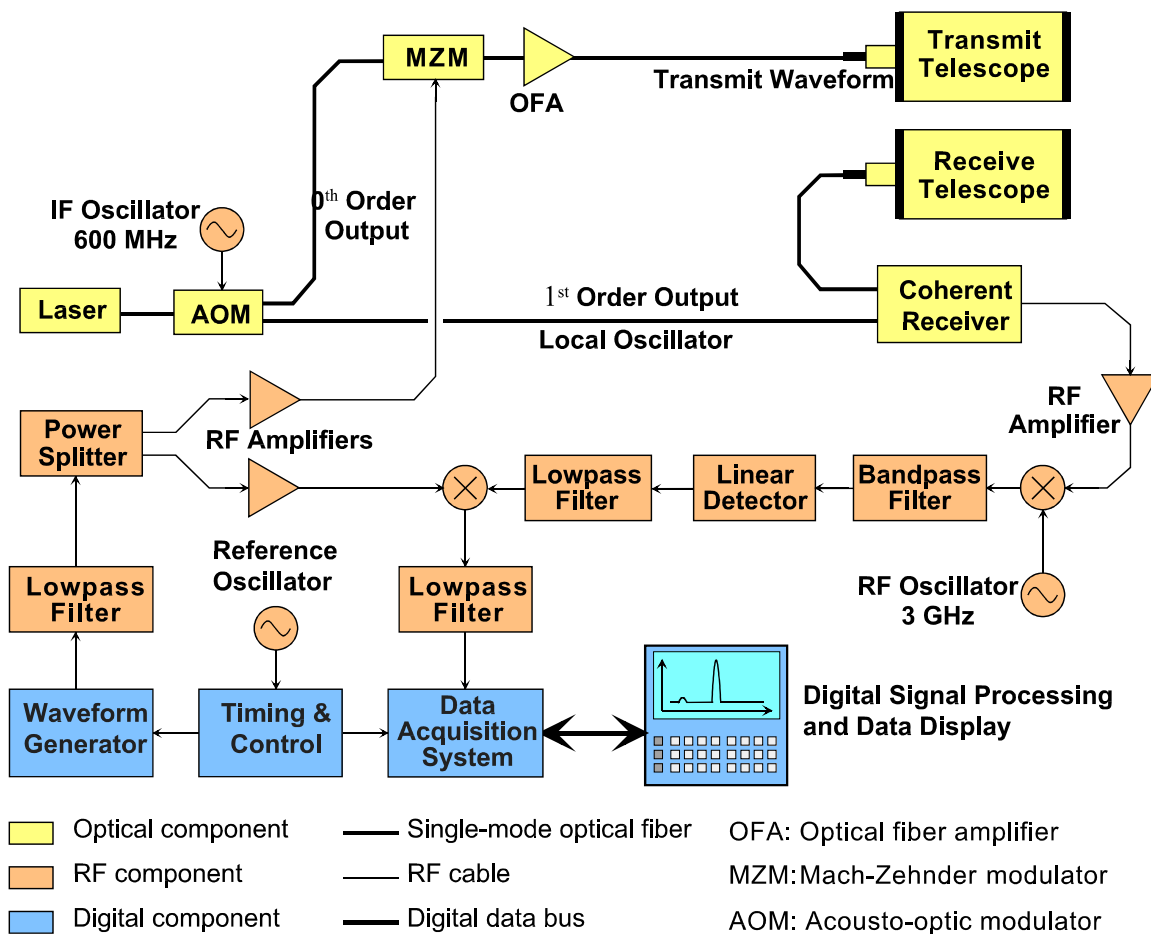


Figure 5.2-1 Block diagram of the system prototype

In the next three sections, we will look at the transmitter, the receiver, and the signal processing sections in detail. We will analyze each component and give their performance parameters.

5.3 The Transmitter

The transmitter of the system consists of a waveform generator, RF components including a 600 MHz oscillator, a low-pass filter, a power splitter, and an RF amplifier and optical components including a 1319 nm wavelength laser source, an acousto-optic modulator (AOM), a Mach-Zehnder modulator (MZM), optical fiber amplifier (OFA) and a transmit telescope. Now we will look at each of these components in detail.

5.3-1 The Waveform Generator: The waveform generator is used to generate a chirp signal with a bandwidth of 260 MHz and a duration of 40 μs . The start frequency of the chirp is 100 MHz and the stop frequency is 360 MHz. This chirp signal is generated every 100 μs giving a 40% duty cycle. The triggering of this signal is handled by the timing and control section so that the generation of this signal is synchronized with the data acquisition system. In our system, the timing and control module is configured so that it makes different components run in synchronization. This task is handled by an 800 MHz oscillator inside the waveform generator.

5.3-2 The RF Section of the Transmitter: This section of the transmitter includes a 600 MHz oscillator, a low-pass filter, a power splitter and an RF amplifier.

a) Oscillator: The oscillator outputs a 600 MHz signal, and this signal drives the AOM, which serves as a frequency shifter. This frequency-shifted light is the local oscillator signal that is input to the coherent receiver. More detail about this will be given during the discussion on the coherent receiver in Section 5.4.

b) Low-pass Filter: The oscillator low-pass filter is used to block high frequency signals coming out of the waveform generator before they enter the power splitter. It has a cut-off frequency of 450 MHz and is used to filter out any harmonics or unwanted signals that might be produced during wave generation.

c) Power Splitter: The power splitter is used to split the incoming signal into two signals. One of those signals is used to drive the Mach-Zehnder modulator (MZM). The other output is used in the receiver section to dechirp the detected signal.

d) RF Amplifier: The RF amplifier is used to amplify the signal coming out of the power splitter before it is used to drive the MZM. Its gain is about 14 dB and it has a noise figure of 3.8 dB.

5.3-3 The Optical Section of the Transmitter: This section of the transmitter includes a 1319 nm wavelength laser source, an acousto-optic modulator (AOM), a Mach-Zehnder modulator (MZM), optical fiber amplifier (OFA) and a transmit telescope.

a) Laser Source: The laser source produces CW light at 1319 nm and has a maximum power output of 20 dBm and a spectral width of 5 kHz. This light is then passed through the AOM and is modulated at the MZM.

b) Acousto-optic Modulator: The AOM is placed after the laser source and is used to split the incoming light into two paths: the 0th order port path and the 1st order port path. The light directed to the 0th order port path (the path for the unshifted light) is the input to the MZM, while the frequency of the light directed to the 1st order port path is shifted down by 600 MHz. This light is then input to the coherent receiver.

c) Mach-Zehnder Modulator: The MZM takes the CW 1319 nm optical signal and intensity modulates it with the chirp waveform.

d) Optical-fiber Amplifier: The OFA is used to amplify the optical signal coming out of the MZM. The gain obtained from this OFA is about 23 dB.

e) Transmit Telescope: The optical tool used to transmit the optical signal is a telescope. Instead of the eyepiece used for traditional telescope applications, a fiber interface is mounted at the back of the telescope. This interface is used to launch light into the telescope through its optics. The telescope has an aperture with a diameter of 127 mm, a focal length of 1.27 m, and an aperture blockage diameter of 0.085 m.

5.4 The Receiver

The receiver of the system consists of a receive telescope, a coherent receiver, two RF amplifiers, two RF mixers, a 3 GHz RF oscillator, a band-pass filter, an envelope detector, and two low-pass filters. Now we will look at each of these components in detail.

5.4-1 The Optical Section of the Receiver: This section of the receiver includes the receive telescope and the coherent receiver.

a) Receive Telescope: The aperture used to receive the light scattered from the target is the same type of telescope described above in the transmitter section. The only difference is in the direction of light, which is from the receiving aperture, through the fiber interface, to the fiber leading to the coherent receiver.

b) Coherent Receiver: The coherent receiver is used to achieve coherent detection of the optical signal scattered from the target. The receiver has two inputs: 1) the light captured by the receive aperture and 2) the light from the AOM that has a frequency shift of 600 MHz with respect to the original optical signal. This frequency-shifted light is called the local oscillator signal and will be used to boost the detected signal power by coherent detection as explained in Section 2.4. These two optical signals are mixed and the output of the coherent receiver is a RF signal. (The photo detector used in this configuration has a noise equivalent power (NEP) of $24 \text{ pA}/\sqrt{\text{Hz}}$.)

5.4-2 The RF Section of the Receiver: This section of the receiver includes two RF amplifiers, a 3 GHz RF oscillator, two RF mixers, a bandpass filter, an envelope detector and two low-pass filters.

- a) RF Amplifiers: The first of the RF amplifiers is placed after the coherent receiver and it boosts the signal power of its output. It provides an amplification of 30 dB, has a noise figure of 5.5 dB and a bandwidth from 50 MHz to 1 GHz. The second RF amplifier is used to boost the signal power of the signal coming out of the second port of the power splitter. It provides an amplification of 15 dB, has a noise figure of 6 dB and a bandwidth from 10 MHz to 4.2 GHz.
- b) 3 GHz Oscillator: The oscillator used in the receiver section produces a 3 GHz signal. Its output is fed into the first mixer to increase the frequency of the signal at its input.
- c) RF Mixers: The first of the RF mixers takes the output of the coherent receiver and upconverts it by 3 GHz using the RF oscillator as its second input. Its output has a frequency 3 GHz higher than the output of the coherent receiver. This is done to provide optimum detection for the envelope detector as it requires a 10:1 or higher ratio between the carrier and envelope frequencies. The second mixer is used to mix the low-pass-filtered output of the envelope detector and the original chirp signal to produce a dechirped signal at its output.
- d) Bandpass Filter: The bandpass filter placed after the RF mixer is included in the receiver configuration to filter out any unwanted harmonics or signals that may be produced during the up conversion of the signal in the previous mixing operation. It has a center frequency of 3.5 GHz and a bandwidth of 1 GHz.
- e) Envelope Detector: The envelope detector has the up-converted signal at its input port as it is used to detect the envelope of this signal. The information about the target's range is obtained from the envelope of this signal, and the frequency information leading to this

range information is obtained after dechirping and signal processing. The envelope of the signal is obtained after low-pass filtering the output of the envelope detector, which is discussed below.

f) Low-Pass Filters: The first of the low-pass filters (LPF) is placed after the envelope detector to obtain the envelope of its input signal. High-frequency terms produced during the envelope detection process are low-pass filtered to obtain the envelope. The second LPF is placed in the path of the dechirped signal to filter out any unwanted signals. The first LPF has a cutoff frequency of 467 MHz while the second one has a cutoff of 10.7 MHz.

5.5 The Signal Processing Section

The signal processing section consists of the data acquisition system and a signal processing and display module. Now we will look at each of these components in detail. (Since the waveform generator outputs the transmitted signal, it has been discussed in the transmitter section.)

5.5-1 The Data Acquisition Module: Once the pulse is transmitted and scattered back from a target, the received signal must be recorded to a data file for analysis. In our system, this task is performed by a data acquisition card placed in a designated computer. This card takes in the incoming data and digitizes them through a 12-bit A/D converter [5]. The rate at which the card can accept data is dependent on the clock frequency. In most of our experiments, we used a 20 MHz clock, so any data rate less than the half of this value is acceptable to the system. (In other words, the sampling frequency is 10 MHz and, to avoid aliasing, the signal frequency should be less than 5 MHz.) For a detailed description of the development and usage of this data acquisition module, see [5].

5.5-2 The Signal Processing and Display Module: Once the data are input to the data acquisition system, necessary signal processing techniques are performed on it. The data acquisition system is capable of performing coherent integrations and FFT on the data.

At the display interface, it is also possible to choose the number of coherent integrations to be performed on the data. When the optimum number of coherent integrations are chosen and the data are ready to be displayed, the FFT is performed. These transformed data are then shown in the data display monitor of the computer together with the time domain representation of the signal. Depending on the clock of the system and the pulse repetition frequency of the transmit signal, the signal shown on the monitor changes to show the new incoming set of data. When the optimum presentation of the data is obtained, the data are recorded for future observations.

5.6 Experiment Results

Once the system prototype was assembled, experiments were carried out to verify the system performance predicted by theoretical analysis and simulations. Below are some of the experiments carried out for this purpose. (Unless specified otherwise, the setup is similar to that given in Figure 5.2-1.)

5.6-1 Results of the Experiment to See the Effects of Changing the Pulsewidth of the

Signal Used: To carry out the experimental testing of the effects of varying pulsewidth, a setup similar to the one given in Figure 5.2-1 is used. One difference is that instead of using the telescopes for transmit and receive, the transmit signal is fed to the receiver through a 20 m fiber-optic cable. This cable simulates the delay that would have been obtained from a scattering target. When the setup is complete, the experiment is carried out to see the improvement obtained in signal-to-noise ratio when the pulsewidth of the chirp used is doubled. For this experiment, the wavelength of operation is 1319 nm. The number of coherent integrations is kept to a low value of 32 to see the effects of doubling the pulsewidth. The different pulsewidths used are 50, 100, and 200 μs . The results are summarized in the table below.

Table 5.6-1: The results for testing the effects of pulsewidth on SNR

Filename	# coh int.	# samples	pw. [us]	BW [MHz]	sig pw[dB]	noise pw[dB]	SNR [dB]
jan21.2	32	1024	50	260	85.26	15.45	69.81
jan21.1	32	2048	100	260	88.5	16.18	72.32
jan21.0	32	2048	200	260	91.1	15.53	75.57

The results seen above suggest that doubling the pulsewidth improves the SNR by 3 dB. The increase is due to the increase in the signal power, and the noise power seems to stay the same. These results agree with the ones predicted by theory, and this can be seen from the gain obtained from the compression ratio in [2.5-5].

5.6-2 Results of the Experiment to See the Effects of Changing the Number of Coherent Integrations on Output SNR and on Minimum Detectable Signal: As

discussed in the theory and simulation sections, performing coherent integrations on the incoming data improves the output SNR. Simulations predicted a 1:1 relationship between the number of coherent integrations and the output SNR. To see if this prediction is valid, an experiment is carried out with our setup. The incoming optical power signal is kept to a low -26.5 dBm to ensure saturation is not reached. Three sets of data are collected at this power level. The first is collected with 256 coherent integrations, the second with 1024 coherent integrations and the third with 2048 coherent integrations. The results are summarized in the table below.

Table 5.6-2: The results for testing the effects of coherent integrations on SNR

# coh. Int.	Output SNR (dB)
256	44.13
1024	51.34
2048	53.71

As seen from Table 5.6-2, increases of 6 dB (4 times) and 3 dB (2 times) are observed in the number of coherent integrations. If the 1:1 prediction is to be validated,

the output SNR should show the same amount of change. The results summarized above show that a four-times increase in the number of coherent integrations increased the output SNR by about 6 dB, while a two-times increase in the number of coherent integrations increased the output SNR by about 3 dB. Thus, the predictions made by the simulations are validated.

Since the SNR is improved by performing coherent integrations, the minimum detectable signal power can also be improved with this method. To test this, four different coherent integration levels of 4, 256, 1024 and 2048 are performed on signals with power levels ranging from -26.4 dBm to -52.4 dBm, and output SNRs are recorded. The results are summarized in the figure given below.

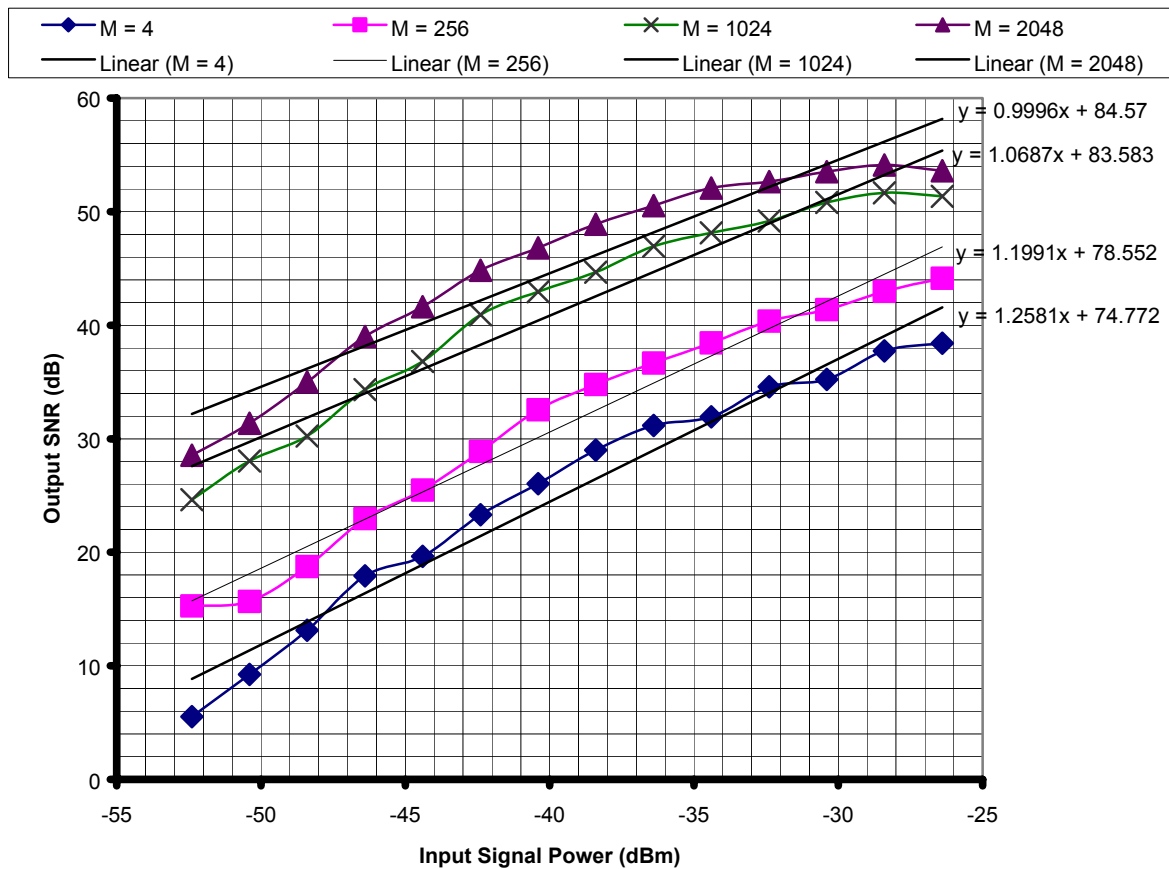


Figure 5.6-2: Results of observing effects of number of coherent integrations on minimum detectable signal.

As seen from the figure above, when the number of coherent integrations (M) is increased, the minimum detectable signal power is decreased. This is evident from the trend shown by the data set with $M=4$. This set reaches its lowest detectable signal value at around -52 dBm, while the other data sets demonstrate the trend that weaker signals can be detected.

5.6-3 Results of the Experiment to See the Relationship Between Input Optical

Power and Output SNR: One of the important relationships in the system is between the input optical signal and the output power (and output SNR). This relationship should be a 1:1 relationship so that the system operates linearly. (For example, if this ratio is 1:2, a 1 dB reduction in input optical signal power would result in a 2 dB drop in the output signal power. This is undesirable.) In order to test if our system works linearly, the input optical signal power is varied in 2 dB steps from -32.4 dBm to -45.7 dBm and the corresponding output SNR is noted. The optical LO power is kept at -13.3 dBm and the number of coherent integrations is set at 256. The results are summarized in Table 5.6-3 and Figure 5.6-3 below.

Table 5.6-3: The results for changing input signal power and noting output SNR.

Input Signal Power (dBm)	Output SNR (dB)
-32.40	47.34
-34.40	44.83
-36.20	43.74
-38.20	41.73
-40.30	38.20
-42.20	38.20
-43.90	35.14
-45.70	32.18

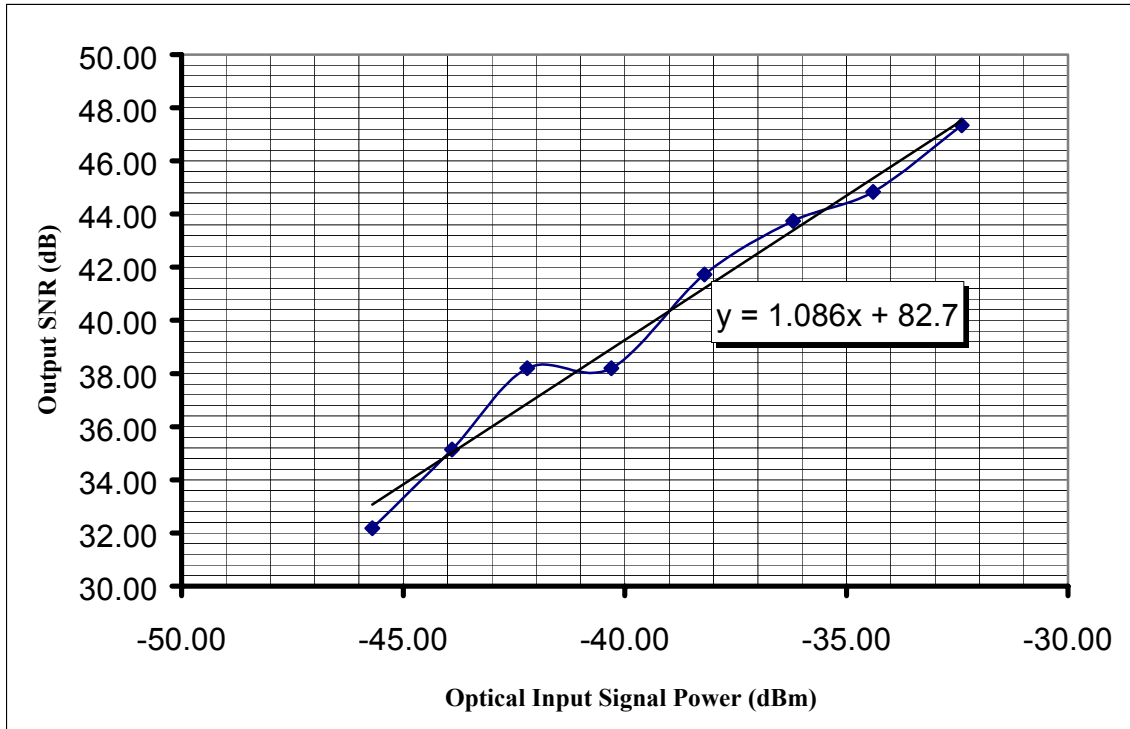


Figure 5.6-3: The plot of results for changing input signal power and noting output SNR.

To better understand the relationship between input optical signal power and output SNR, the plot above can be observed. It contains the plot of the data collected together with a fitted line that shows the linear relationship between the two variables in question. This relationship is seen in the equation $y = 1.086x + 82.7$ (where y represents output SNR and x stands for input power) and the 1:1 relationship desired is validated. This means that for every 1 dB change in input optical signal power, there will be corresponding 1 dB change in output SNR.

5.6-4 Minimum Detectable Optical Input Signal Power Experiment: Once the system's linearity is validated (as seen in previous section), it is important find the system's minimum detectable optical signal power. In other words, we need to find the power level for the weakest signal input to the receiving aperture that can be detected in the data collection module. To achieve this goal, the settings for parameters such as LO power and number of coherent integrations are set at their optimum values, and the

signal power is decreased until the signal cannot be detected in the data collection module.

The starting point for the signal power is chosen to be -52.6 dB where a strong SNR is seen. The LO power is fixed at 0 dBm and the number of coherent integrations is set at 256. The results of the experiment are summarized in Table 5.6-4 and Figure 5.6-4 below.

Table 5.6-4: The results for finding minimum detectable optical input power.

Input Signal Power [dBm]	SNR [dB]
-52.6	43.14
-54.6	41.86
-56.6	39.44
-58.6	39.58
-60.6	40.85
-62.6	40.88
-64.6	38.3
-66.6	37.41
-68.6	32.89
-70.6	29.92
-72.6	23.97
-74.6	20.66
-75.6	24.51
-76.6	20.36
-77.6	22.18
-78.6	19.73
-79.6	15.98
-80.6	19.78
-81.6	14.88
-82.6	15.98
-83.6	11.94
-84.6	12.38
-85.6	3.39
-86.6	10.65
-87.6	3.2
-88.6	9.05
-89.6	9.28
-90.6	9.76
-91.6	2.67

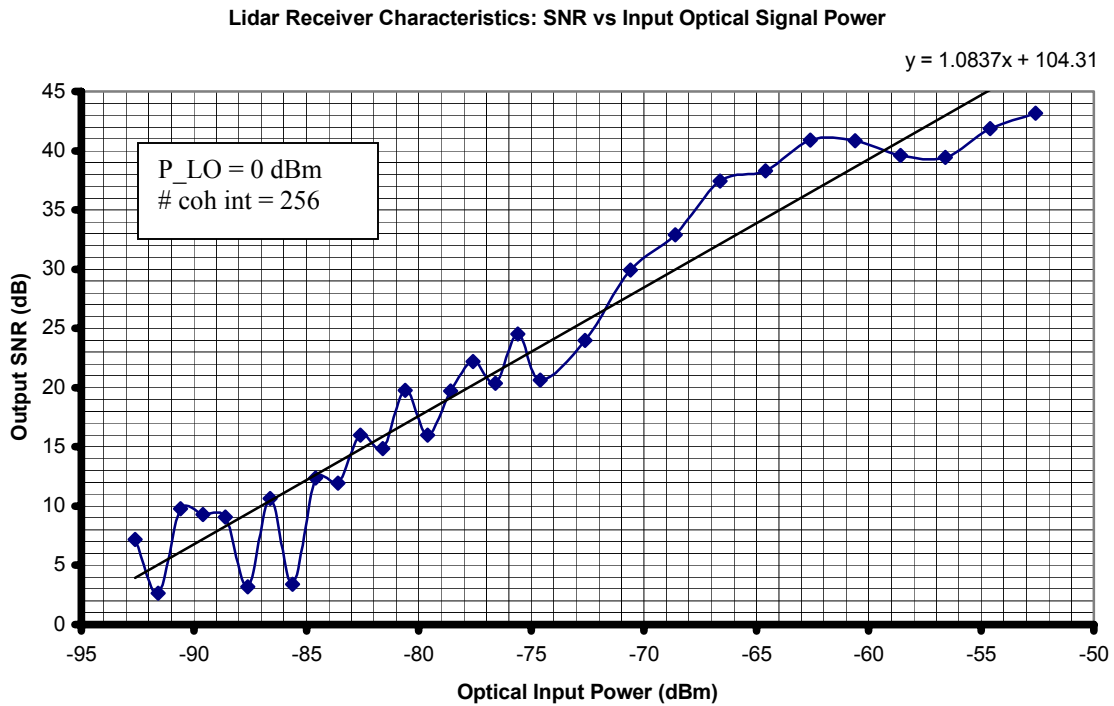


Figure 5.6-4: Plot of results for finding the minimum detectable optical signal power.

As seen from the results above, the lowest value for an incoming signal for detection is around -92 dBm. However, we should keep in mind that this value is only valid for this setup and set of values for parameters such as LO power. If any of these settings are changed, this value will be different.

The plot also shows fluctuations in SNR at low input power levels. This effect is thought to be due to noise dominating in some instances. When the input power levels are low, the random effects of noise are more dominant, changing the SNR in a non-uniform manner.

5.7 Conclusions

In this fifth chapter, a system prototype was presented and each of its components was discussed. Once the system description was complete, the results of experiments carried out with this prototype were presented. These experiments help predict system performance and verify results predicted by calculations and simulations.

The system described has transmitter, receiver and signal processing parts with the signals in these sections being either in the optical or the RF domain. Once we described these components, we discussed testing of the system's performance and presented the results of these tests.

First we present the results of changing the pulsewidth of the transmit signal we used. We used three pulsewidths of 50, 100 and 200 μs and noted the SNR. As expected, the SNR increased by 3 dB when the pulsewidth was doubled. Next we discuss the results of changing the number of coherent integrations to see their effect on SNR and the minimum detectable signal. The three sets of data were collected with 256, 1024 and 2048 coherent integrations and the SNR is noted. The results show that there is a 1:1 relationship between SNR and an increase in the number of coherent integrations. Increasing the number of coherent integrations also decreases the minimum detectable signal as the SNR is improved without a need to increase the transmit power. We also tested the relationships between the input optical power and output SNR. The input signal power is varied by 2 dB from -45.7 to 32.4 dBm and the output SNR is noted. Once the results are plotted, we see a 1:1 relationship between the two quantities in questions. Finally, we measured the minimum detectable optical input signal for this system by systematically reducing the input optical signal power until the system could not detect the target scattering. The results of this experiment show that the minimum detectable optical input signal is around -92 dBm.

The next chapter introduces additional system configurations we tested to achieve better system performance.

CHAPTER 6

Other System Configurations

6.1 Introduction

In this section, additional system configurations will be presented. Although the transmitter, receiver and signal processing main sections will still be used, changes will be made within each section. This is to see if better system performance can be obtained.

The two variations discussed in this chapter are homodyne versus heterodyne configuration and inphase-quadrature detection with direct down conversion.

6.2 Homodyne versus Heterodyne Detection

In this section, additional system configurations will be presented. Although the transmitter and receiver principles are basically the same as before, a few changes are made. For the homodyne detection case, the system configuration is different since the acousto-optic modulator is removed from the system. This is done to avoid the insertion loss of this component. Without the acousto-optic modulator, the optical signal transmitted does not have the 600 MHz frequency difference from the optical signal at the receive end of the system. Figure 6.2-1 shows the homodyne system configuration.

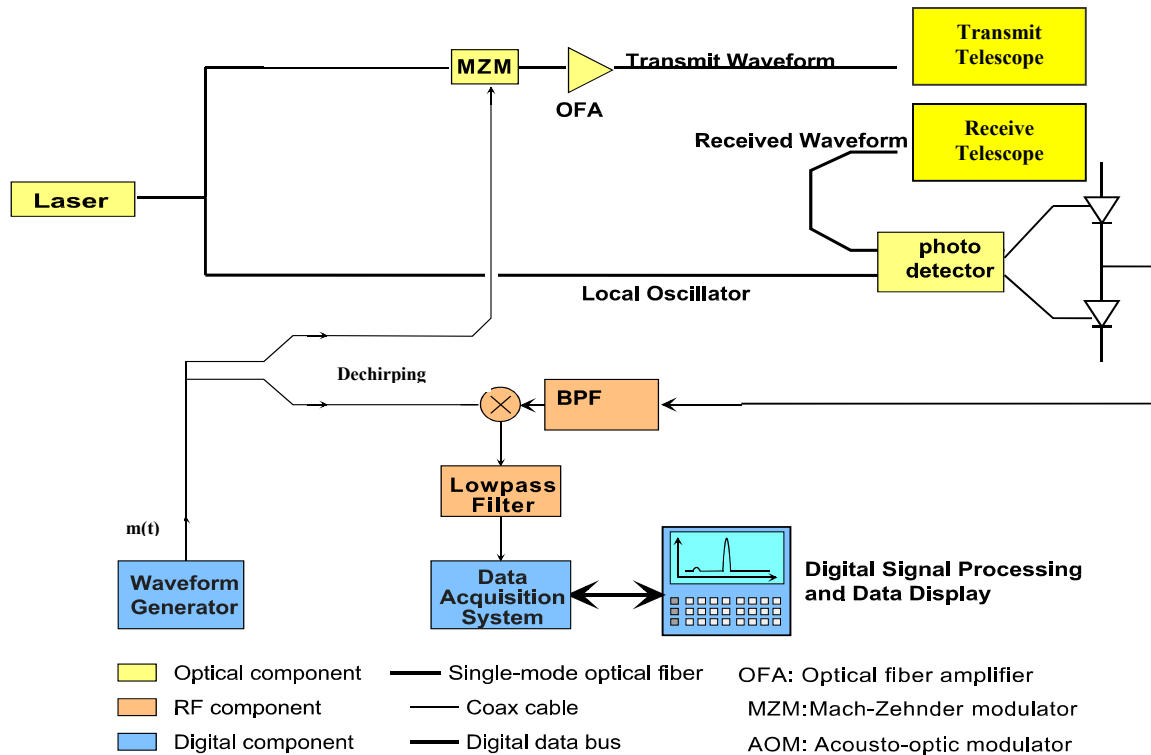


Figure 6.2-1 Homodyne system configuration.

As seen from the figure above the homodyne system's configuration differs from that of the heterodyne system because no 600 MHz shift has been made on the transmit signal and hence no LO signal is used.

When the above configuration was implemented and tested, the system performance was not satisfactory. This was due to the optical phase variations at the photodiode causing the received signal to be unstable. When the phase was aligned the output was satisfactory, while when not aligned the signal was lost. To eliminate this effect, a 3-by-3 coupler could be used. Each output of the 3-by-3 coupler would have a photo detector and each channel would have to be processed separately. This solution increases the hardware needed and hence was undesirable.

6.3 Inphase Quadrature with Direct Downconversion

In this section, the inphase quadrature with direct down conversion (I&Q-DDC) method is implemented and tested to see if the fluctuations in the receive signal due to phase variations can be reduced or eliminated. The figure below shows the configuration used for this method.

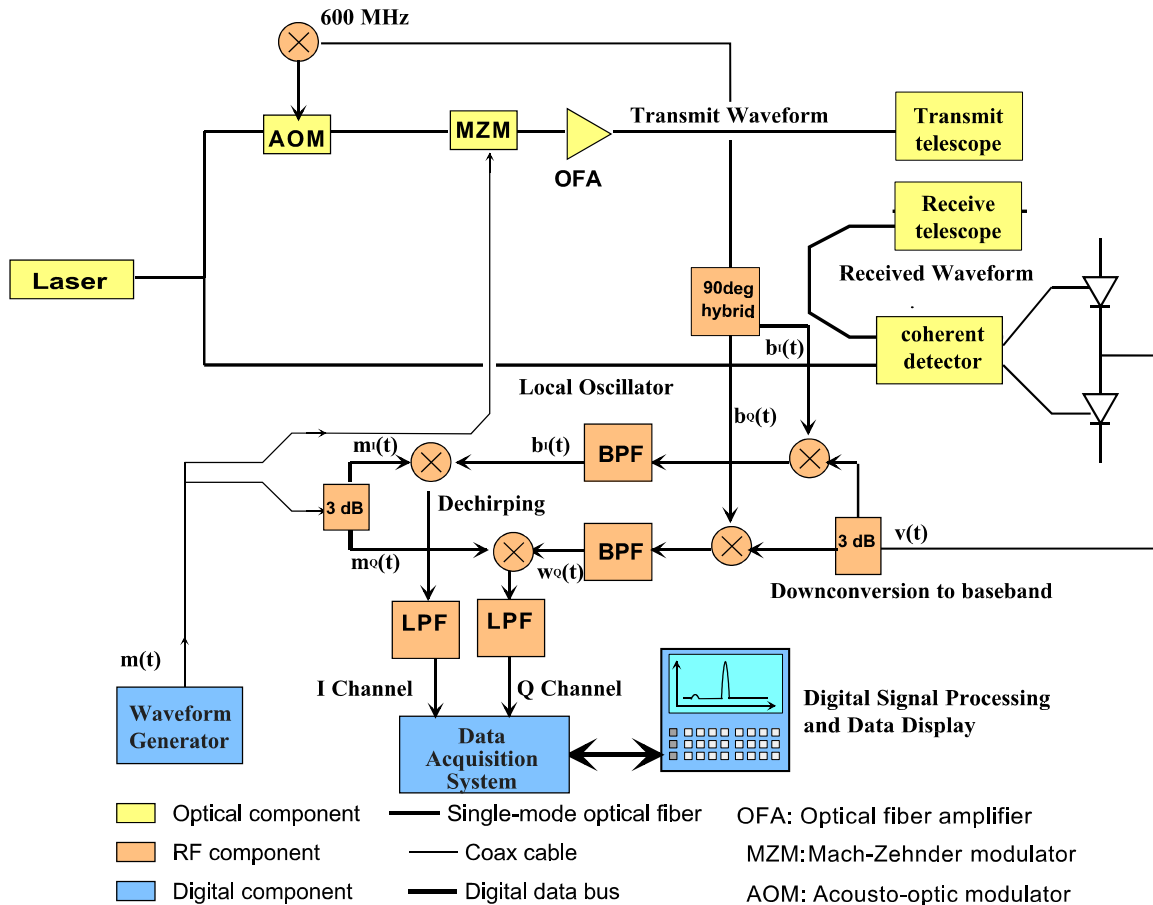


Figure 6.3-1 I&Q-DDC system configuration.

As seen in the figure above, the optical part of the system is the same as the heterodyne configuration in the sense that the AOM is used to provide the 600 MHz shift in the optical transmit path. A coherent detector is in place followed by down conversion. After the photo detector some changes are also made to eliminate the phase variations seen in the received signal.

The signal at the output of the photo detector is $v(t)$ and its mathematical representation is given below:

$$v(t) = A[1 + m(t - \tau)] \cos(-2\pi f_{TX} \tau + 2\pi f_s t + \phi_{IF}) \quad [6.3-1]$$

where

A = Amplitude of the received signal [Volts]

τ = Time delay from the target [seconds]

$m(t - \tau)$ = Function denoting the time-delayed chirp

f_{TX} = Frequency of the transmitted signal [Hz]

f_s = Local oscillator frequency [Hz]

ϕ_{IF} = Phase of the received signal [rad/s]

The signal in [6.3-1] is split into two equal parts through a 3-dB splitter to obtain $v_i(t)$ and $v_o(t)$, which are identical. The 600 MHz local oscillator signal, $b(t)$, is also split in two through a 90° hybrid. This split presents a 90° phase difference to one of the two local oscillator signals. The local oscillator signal, $b(t)$, and the two LO signals, $b_i(t)$ and $b_o(t)$, are shown below:

$$b(t) = 2 \cos(2\pi f_s t) \quad [6.3-2a]$$

$$b_i(t) = \cos(2\pi f_s t) \quad [6.3-2b]$$

$$b_o(t) = \cos(2\pi f_s t) e^{j90} = \sin(2\pi f_s t) \quad [6.3-2c]$$

At this point the signal, $v_i(t)$, is multiplied with LO signal, $b_i(t)$, to obtain $w_i(t)$ while $v_o(t)$ is multiplied with $b_o(t)$ to obtain $w_o(t)$.

These two signals are shown below:

$$w_i(t) = \frac{v(t)}{2} b_i(t) = \frac{A}{2} [1 + m(t - \tau)] \cos(-2\pi f_{TX} \tau + 2\pi f_s t + \phi_{IF}) \cos(2\pi f_s t) \quad [6.3-3a]$$

$$w_o(t) = \frac{v(t)}{2} b_o(t) = \frac{A}{2} [1 + m(t - \tau)] \cos(-2\pi f_{TX} \tau + 2\pi f_s t + \phi_{IF}) \sin(2\pi f_s t) \quad [6.3-3b]$$

Using trigonometric identities for the multiplication of trigonometric functions, the following representations are obtained for $w_i(t)$ and $w_o(t)$:

$$w_i(t) = \frac{A}{2} [1 + m(t - \tau)] \frac{1}{2} [\cos(\text{double freq. term}) + \cos(-2\pi f_{TX} \tau + \phi_{IF})] \quad [6.3-3c]$$

$$w_o(t) = \frac{A}{2} [1 + m(t - \tau)] \frac{1}{2} [\sin(\text{double freq. term}) - \sin(-2\pi f_{TX} \tau + \phi_{IF})] \quad [6.3-3d]$$

The two terms resulting from the multiplication of the two trigonometric functions yield two signals, one having a frequency equal to the addition of the two frequencies, while the second term has a frequency equal to the subtraction of two frequencies. Since the term with the double frequency (addition of frequencies) is not needed, it is filtered out using a bandpass filter and the following representations are obtained:

$$w_{i\text{bp}}(t) = \frac{A}{4} [m(t - \tau)] [\cos(-2\pi f_{TX} \tau + \phi_{IF})] \quad [6.3-4a]$$

$$w_{o\text{bp}}(t) = \frac{A}{4} [m(t - \tau)] [-\sin(-2\pi f_{TX} \tau + \phi_{IF})] \quad [6.3-4b]$$

As seen from [6.3-4a & b], when the terms in the cosine function add to 90° or when the terms in the sine function add to 0° , the entire function reduces to zero. Also, the variations to the phase term cause the amplitude of this signal to vary. This is the reason that the I&Q-DDC method is applied to eliminate the effects of phase variation.

The next step is dechirping. At this stage, the chirp signal is also split into two equal parts through a 3 dB splitter. These two identical chirp signal are shown below:

$$m_i(t) = m_o(t) = a \cos(2\pi f_c t + 0.5 k t^2) \quad [6.3-5]$$

where

a = amplitude of the chirp [V]

f_c = chirp start frequency [Hz]

k = chirp rate $[\frac{\text{MHz}}{\mu\text{s}}]$

These two chirp signals are then multiplied with the signals given in [6.3-4a and b]. The resulting signals are shown below:

$$x_i(t) = w_{i\text{bp}}(t) m(t) = \frac{A}{4} [m(t-\tau)] [\cos(-2\pi f_{\text{TX}} \tau + \phi_{\text{IF}})] m(t) \quad [6.3-6a]$$

$$x_o(t) = w_{o\text{bp}}(t) m(t) = \frac{A}{4} [m(t-\tau)] [-\sin(-2\pi f_{\text{TX}} \tau + \phi_{\text{IF}})] m(t) \quad [6.3-6b]$$

After this multiplication is complete, the results have a chirp-squared term that is not useful. So $x_i(t)$ and $x_o(t)$ are filtered to get rid of the chirp-squared term and the signals shown below are obtained:

$$y_i(t) = \frac{A}{4} \left[\frac{a^2}{2} \cos(2\pi f_c \tau + k\tau t - 0.5k\tau^2) \right] [\cos(-2\pi f_{\text{TX}} \tau + \phi_{\text{IF}})] \quad [6.3-7a]$$

$$y_o(t) = \frac{A}{4} \left[\frac{a^2}{2} \cos(2\pi f_c \tau + k\tau t - 0.5k\tau^2) \right] [\sin(-2\pi f_{\text{TX}} \tau + \phi_{\text{IF}})] \quad [6.3-7b]$$

Once these signals are at hand, an FFT is performed to get the frequency information and then they are squared to obtain power vectors and added together to obtain the received signal, $y(t)$, to be processed. The range information will be obtained from the beat

frequency term, $k\tau$. Since the sine and cosine terms are simply weights, when y_i and y_o are squared and added, they will sum to 1. Hence, the effect of ϕ_{if} is eliminated.

Once the signal's dependence on phase variations is eliminated, the receiver's sensitivity is measured. This is done by measuring the minimum detectable signal. The following table and figure show the results of this experiment. The number of coherent integrations is one, the number of samples is 2048 and the LO power is 0 dBm.

Table 6.3-1 I&Q-DDC system minimum detectable signal measurement.

Signal Power out of attnr [dB]	Attenuation[dB]	Pout (I+Q)[dB]	Pnoiseout [dB]	SNRout [dB]
-71	30	75.75	46	29.75
-73	32	74.11	46	28.11
-75	34	71.69	46	25.69
-77	36	69.76	46	23.76
-79	38	69.28	46	23.28
-81	40	65.27	46	19.27
-83	42	64.24	46	18.24
-85	44	61.17	46	15.17
-87	46	60.36	46	14.36
-89	48	58.16	46	12.16
-91	50	56.5	46	10.5
-93	52	56.3	46	10.3
-95	54	52.69	46	6.69

As seen from the data presented above the minimum detectable signal for the I&Q DDC system is about -95 dBm. This can also be seen from the graph of these data given below.

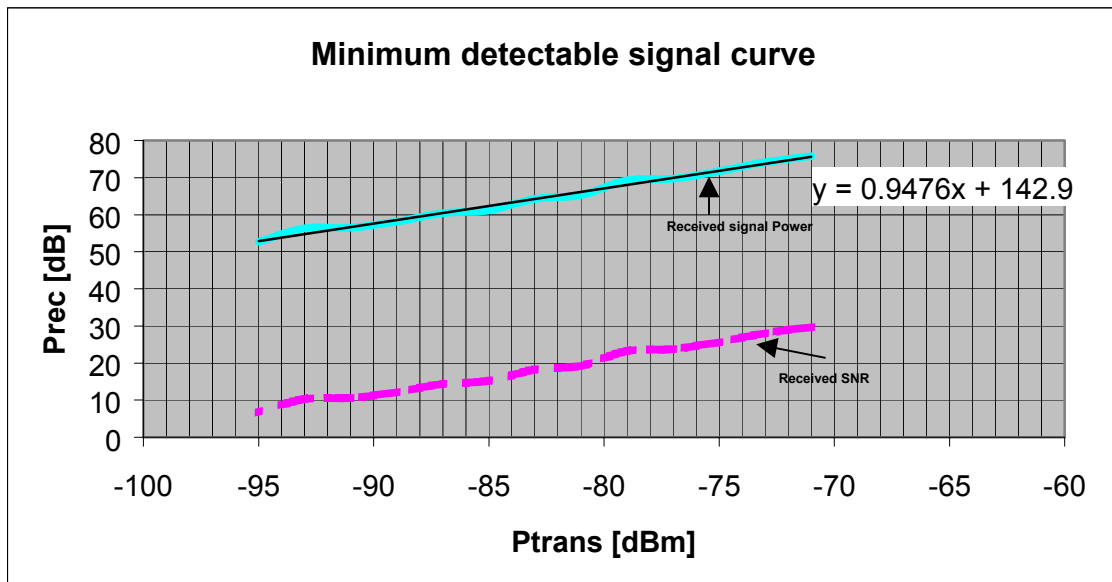


Figure 6.3-2 I&Q-DDC system minimum detectable signal plot.

The above plot not only shows the minimum detectable signal to be around -95 dBm but also shows that the 1:1 relationship between the transmit and received signals is also maintained with the new system, as shown by the equation of the fitted line.

Once the minimum detectable signal is determined, detection of a Lambertian target should be demonstrated. This is done in the following experimental setup. The target to be detected is snow on asphalt, approximately 20 m from the telescope. This setup is shown in Figure 6.3-3. The transmit power is 14.6 dBm, the LO power is 0 dBm, pulsewidth is 200 μ s and the aperture diameter of the telescope used is 5 in. Figure 6.3-4 shows the plot of the data collected.

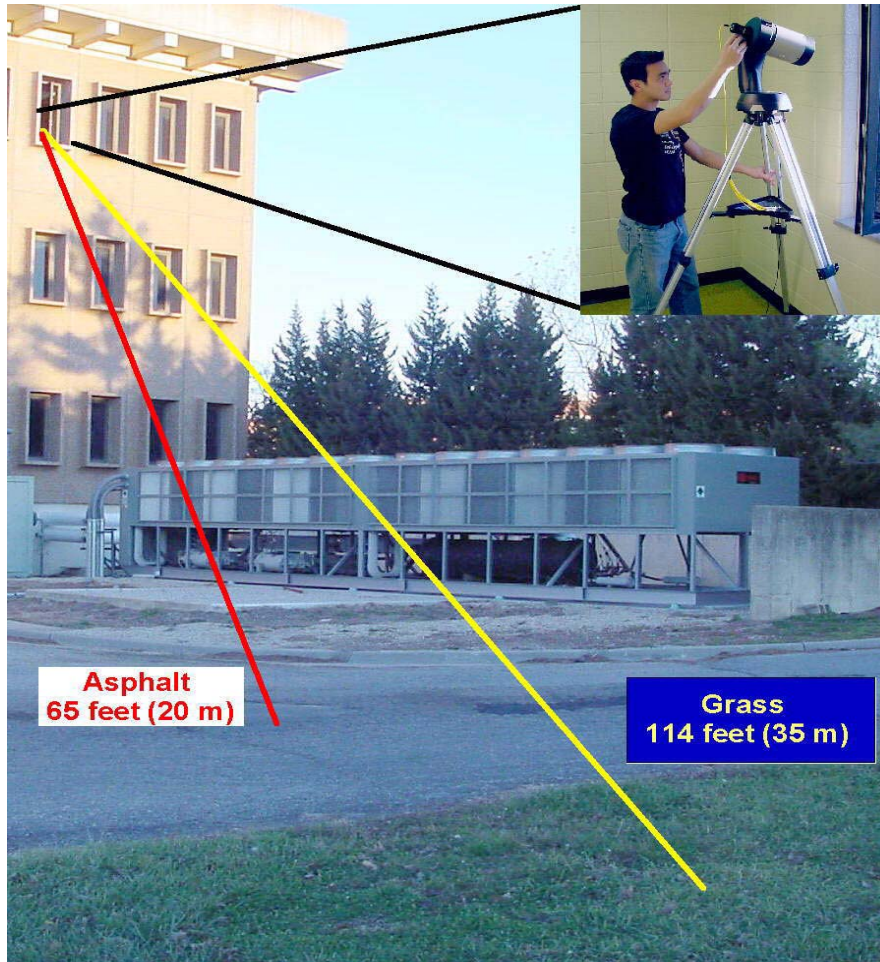


Figure 6.3-3 Picture showing the distance to the target at 20 m (Red Line)

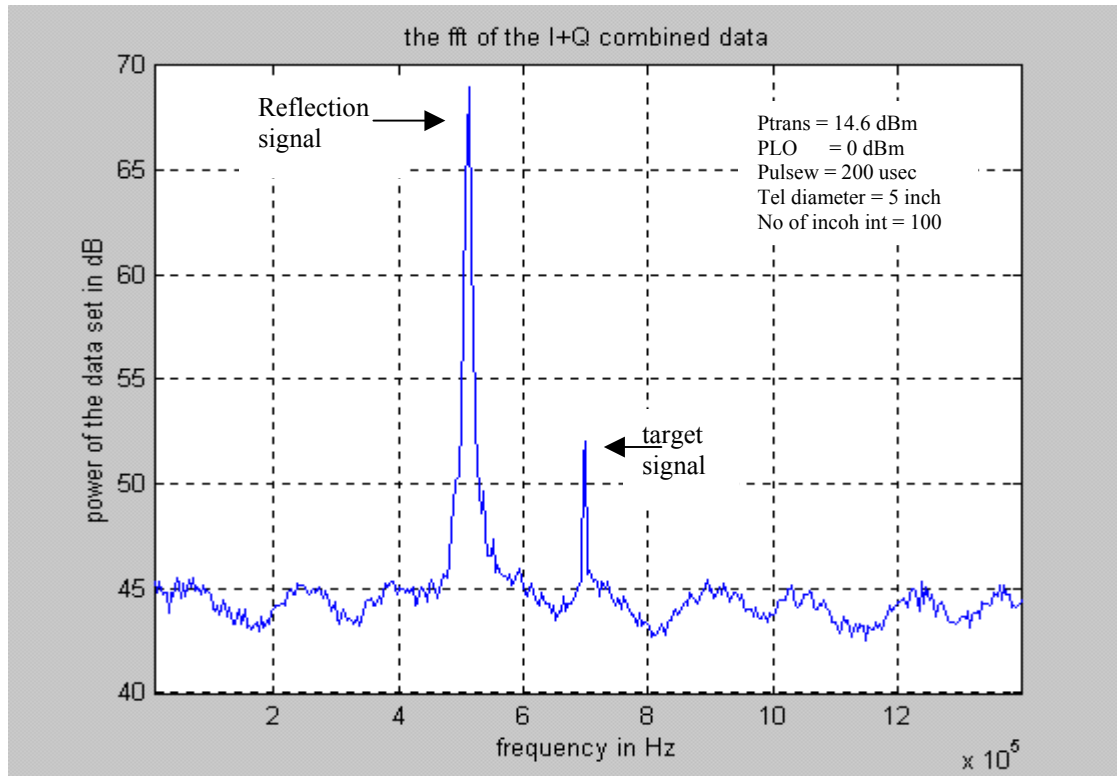


Figure 6.3-4 Plot of the data collected with snow as target

The first spike seen in this graph is from the internal reflection from the telescope. It occurs at a frequency of 511.72 kHz. The second spike corresponds to the reflection from snow. This signal occurs at a frequency of 699.22 kHz and has a power of 53 dB. The noise power is about 43 dB. By using the frequency of the reflection together with the frequency of the target, the distance to the target can be found. This calculated distance corresponds to a distance of 21.6 m. (Since the data collected were intended only for the proof of detection, the calculated distance and the measured distance will not be compared for range accuracy.)

When the results above are observed, the I&C DDC technique shows promise. Further investigation of this technique is necessary to improve its performance for detection of Lambertian targets at longer distances.

CHAPTER 7

Conclusion and Future Recommendations

In the previous six chapters, the implementation of a laser radar system was discussed in detail. First, general information about the objectives of the project were presented. Next was the theoretical proof of the concepts to be implemented. This included showing how pulse compression, coherent detection and coherent integrations dramatically improved receiver sensitivity. Then, using a block diagram, the implementation of the proposed system was shown. To predict the performance of the system, simulations were carried out and results presented. To test system performance, selected variables were changed to see their effects on important system parameters like the minimum detectable input signal. These variables were local oscillator power, NEP, and modulation index.

Next a system prototype was put together using standard components. After explaining the functions of major parts of the prototype, the results of the test of system performance were presented. System variables like pulsewidth and coherent integrations were varied to perform systems tests. With envelope detection, system minimum detectable signal power was measured to be around -92 dBm.

Other techniques, homodyne detection and I & Q detection schemes, were also tested. The I & Q scheme improved linearity of the system and had a minimum detectable signal power of -95 dBm.

Future tests for the system should include more system performance tests with the I & Q configuration. Improving fiber-to-telescope coupling efficiency is also important. At this stage, the system has a one-way loss of about 20 dB. Since the theory suggests it could be as low as 5 dB, looking for ways to reduce losses through the transmit-receive telescope is necessary. Also more tests should be carried out to see if a collimated or focused transmit signal gives the better performance.

For the heterodyne system configuration, the frequency drift between the transmit signal and the local oscillator signal is undesirable. Frequency-locking lasers that provide these signals also require investigation. An alternative to the heterodyne configuration is the homodyne configuration. When the homodyne configuration was tested, the performance was unsatisfactory. This was due to the optical phase variations at the photodiode causing the received signal to be unstable. When the phase was aligned the output was satisfactory, while when not aligned the signal was lost. Further investigation of this configuration might yield a more satisfactory system performance.

Other areas of future work could be investigating the benefits of excess pulsewidth, operation in FM-CW mode and the use of large-core multimode fiber instead of single-mode fiber. Finally a scanner configuration, where the transmitted signal scans an area rather than a point, is suggested.

References

- [1] United Nations Environment Programme, Information Unit for Conventions (IUC), Climate Change Information Sheet 5, “How will the climate change?,” <http://www.unep.ch/iuc/submenu/infokit/fact05.htm>.
- [2] Thomas, R. H., “Ice sheets “ in Gurney, R. J., J. L. Foster, & C. L. Parkinson, eds., *Atlas of Satellite Observations Related to Global Change*, Cambridge University Press, Cambridge, England, 1993.
- [3] Allen, C., Y. Cobanoglu, S. K. Chong, & S. Gogineni, “Development of a 1310-nm, coherent laser radar with RF pulse compression,” *Proc. Of 2000 International Geoscience and Remote Sensing Symposium (IGARSS'00)*, Honolulu, Hawaii, pp. 1784-1786, July 2000.
- [4] Jelalian, A. V., *Laser Radar Systems*, Artech House, Norwood, Massachusetts, 1992.
- [5] Akins, T. L., *Design and Development of an Improved Data Acquisition System for the Coherent Radar Depth Sounder*, MS. Thesis, also Radar Systems and Remote Sensing Laboratory Technical Report 13720-9, University of Kansas, November 1998.
- [6] Powers, J., *An Introduction to Fiber Optic Systems*, R. D. Irwin Publishing, a Times Mirror Higher Education Group, Inc., Chicago, 1997.

APPENDIX

APPENDIX A

Matlab Program used for Simulations

```

%*****
%
% This program is used to predict the performance
% of the laser radar system.
% Changes are made when different variables are to be
% tested
%
% DATE:06/26/2000
%*****

clear
clc

% Getting user input for input signal power
% -----

pwr_in_dBm = input(' \n Incoming Power in dBm\n');
pwr_in = 10^((pwr_in_dBm-30)/10);
Vinpp = (sqrt(2*pwr_in));          % Input signal amplitude

% Setting the power level for the LO signal
% -----

Pwr_lo_dBm = 0;                    % LO power (dBm)
Pwr_lo = 10^((Pwr_lo_dBm-30)/10); % LO power in (W)
Vrms_lo = sqrt(Pwr_lo*2);
Vpp_lo = Vrms_lo*(sqrt(2))*2;      % LO Amplitude

% Below delay amount is assigned for the multiplication
% of the chirp & its delayed version & the delay vectors
% are formed
% -----

z_s1=10000;                         % delay amount
z_s2 = 20000 - z_s1;
add1 = zeros(1,z_s1);               % delay vector 1
add2 = zeros(1,z_s2);               % delay vector 2

% Getting user info for number of coherent integrations
% to be performed
% -----

av = 1;          % no. times to average

```

```

% This portion sets the offset frequency for the LO
% -----

    delta =600; % offset frequency for the LO in MHz

% Initializing the presum array to be used in averaging
% -----

    presum1 = zeros(1,120000);

% Constants
% -----

    pulsewidth = 1e-5;           % 10 usec
    bandwidth = 2.6e8;           % 260 MHz
    k = bandwidth/pulsewidth;    % chirp rate [Hz/s]
    w = 2*pi*100e6;             % start frequency [rad/s]
    i = 1:1e5;
    imax =max(i);
    dt = 1e-10;                 % time increment [s]

    t = i*dt;                   % time [s]
    tmax = max(t);
    BW = 1/tmax;                % beamwidth per bin
    ka = 0.9;                   % modulation amplitude sensitivity
    Am = 1;                     % amplitude of modulating chirp
    mi = ka*Am;                 % modulation index

    Resp = 1;                   % Responsivity of reciver[A/W]
    NEP = 2.0e-11;              % Noise equiuv power [A/(Hz)^.5]
    BW_rec = 800e6;             % Receiver BW [Hz]
    q = 1.6e-19;                % Electron Charge [Columbs]

    Fmax = 1/dt;
    N = length(t);
    dF = Fmax/N;                % Frequency spacing [Hz]
    F = dF*i;                   % Frequency Array

% Creating the chirp in the time domain
% -----

    chirp = Am*cos((w*t) + (.5*2*pi*k*t.*t));

```

```

% Defining the carrier and LO frequency
% -----

w_car = 2*pi*2e9;
offset_freq = delta*1e6;
w_LO = w_car + (2*pi*offset_freq);

% Creating the modulated return signal
% -----

y_ret = (0.5*Vinpp)*(1+(mi*chirp)).*cos(w_car*t);

% Creating the LO signal
% -----

y_LO1 = sin(w_LO*t);
y_LO = Vpp_lo*y_LO1;

% Creating the noise array amplitudes
% -----

% Creating the thermal noise vector amplitude
% -----

P_N_opt = (NEP*(sqrt(BW_rec)))/Resp;
P_Noise_th = (P_N_opt*Resp)^2;

% factor to account for the BW difference(F_sample vs.
% receiver BW)

noiseBW_corr_fac = 1/sqrt(2*BW_rec*dt);
V_Noise_ther = noiseBW_corr_fac*sqrt(P_Noise_th);

% Creating the shot noise vector amplitude
% -----

P_N_shot = 2*Resp*q*BW_rec*(Pwr_lo + pwr_in);
P_Noise_shot = (P_N_opt*Resp)^2;

% factor to account for the BW difference(F_sample vs.
% receiver BW)

noiseBW_corr_fac = 1/sqrt(2*BW_rec*dt);
V_Noise_shot = noiseBW_corr_fac*sqrt(P_Noise_shot);

```

```

% Mixing the LO and the modulated signal
% -----

    y = y_LO + y_ret;

% Photo-Detection process
% -----

    za = y.*y;

% Removing the DC content
% -----

    za_avg = mean(za);
    za = za - za_avg;

    testing = []; % creating an empty array for later use
    st = 1;      % for freq domain averaging case

% Here user input is asked to see if signal, noise or
% signal+noise should be processed and displayed
% -----

    display('Below is the choice for what to input to
            system')

    choice = input('(1)Signal only, (2)Noise only,
                   (3)Sig+Noise');

% Defining the filters used in the system
% -----

% Defining filter #1
% -----

    N1 = 79;           % Order of the filter
    Oc11 = 0.106;     % The start frequency [106 MHz]
    Oc21 = 1.07;     % The stop frequency [1.07 GHz]

    Wn1 = [Oc11/5 Oc21/5];
    b1 = fir1(N1,Wn1); % Forming the filter

```

```

% Defining filter #2 [Used to filter the up-converted
% signal]
% -----

N2 = 79;           % Order of the filter
Oc12 = 3.1;       % The start frequency [3.10 GHz]
Oc22 = 4.07;     % The stop frequency [4.07 GHz]

Wn2 = [Oc12/5 Oc22/5];
b2 = fir1(N2,Wn2); % Forming the filter

% Defining filter #3 [Used to filter the linear detector
% output]
% -----

N3 = 79;           % Order of the filter
Oc13 = 0.05;     % The start frequency [DC]
Oc23 = 1.07;     % The stop frequency [1.07 GHz]

Wn3 = [Oc13/5 Oc23/5];
b3 = fir1(N3,Wn3); % Forming the filter

% Creating the 3 GHz signal to be used in Up converting
% the detected signal
% -----

threegig = sin(2*pi*3e9*t);

% Getting user input as to the number of integrations to
% be performed
% -----

rr = input('How many times to average the detected
           signal: ');

```

```

% the For Loop that will perform the addition of the
% desired amount of vectors
% -----

    for ii = 1:rr,
        ii

% Creating the noise arrays (created in the FOR loop to
% have random arrays each time
% -----

        noise1 = randn(size(y_ret));
        noise2 = randn(size(y_ret));
        noise_ther = V_Noise_ther*noise1;
        noise_shot = V_Noise_shot*noise2;
        noise = noise_ther + noise_shot;

% Square-law detecting the signal and adding noise
% -----

        if choice == 1          % If choice is to only see signal
            z = za;

        elseif choice == 2     % If choice is to only see noise
            z = noise;

        N = 79;                % Optimum order to filter
        Oc1 = 0.16;            % start freq
        Oc2 = 2.57;           % stop freq

        Wn = [Oc1/5 Oc2/5];
        b = fir1(N,Wn);

        z_BWfilt = filter(b,1,z);

% Looking at noise power in the time domain
% -----

        VzBWfilt = (abs(z_BWfilt));
        power_in_zBWfilt = VzBWfilt.*VzBWfilt;

        display('This power is good for only noise power')
        avg_pinz_BWfilt = mean(power_in_zBWfilt)

```

```

elseif choice == 3 % If the choice is signal & noise

z = za + noise;

end

% Using Filter 1 (multiple filters used to get better
% rejection)
% -----

z1f = filter(b1,1,z);
z2f = filter(b1,1,z1f);
z_filt = filter(b1,1,z2f);

% Getting rid of the DC Component
% -----

dc_comp = mean(z_filt);
z_filt_nodc = z_filt - dc_comp;
z_filt_nodc(1:200) = (z_filt_nodc(501:700));

% Up-converting the signal by 3 GHz
% -----

z3gig = z_filt_nodc.*threegig;

% Using Filter 2
% -----

z3g_filt = filter(b2,1,z3gig);

% Looking at the average power at this point
% -----

V_mult = (abs(z3g_filt));
power_in_V_mult = V_mult.*V_mult;
avg_pinV_mult = mean(power_in_V_mult)

% Linear detection
% -----

rect_z3gbp1 = 0.5*(z3g_filt + abs(z3g_filt));
rect_z3gbp1(1:10) = rect_z3gbp1(101:110);

```

```

% Using filter 3
% -----

    rect_z3gfilt = filter(b3,1,rect_z3gbp1);

% Making the average 0
% -----

    avg = mean(rect_z3gfilt);
    rect_z3gfilt = rect_z3gfilt - avg;
    avg_after = mean(rect_z3gfilt);

% Dechirping Process
% -----

% Creating the time delayed version of the chirp
% -----

    delay_chirp = [add1 add2 chirp];

% Creating the delayed version of the return signal
% -----

    z_delay = [add1 rect_z3gfilt add2];

% Multiplying the two signals(original and returned)
% -----

    mult = z_delay.*delay_chirp;

% Defining a new set variables for plotting (since array
% size increased from 100000 to 120000
% -----

    inew = 1:1.2e5;
    inewmax = max(inew);
    dtnew = dt;
    tnew = inew*dtnew;
    Fmaxnew = 1/dtnew;
    Nnew = length(tnew);
    dFnew = Fmaxnew/Nnew;
    Fnew = dFnew*inew;
    Nplot = Nnew/12;
    tem = Fnew;

```

```

    for j=1:(inewmax-1),
        Fnew(j+1) = tem(j);

    end

    Fnew(1) = Fnew(2) - dFnew;

% Taking the FFT of the dechirped signal
% -----

    presum_fft = fft(mult);
    mag_presum = abs(presum_fft) / (sqrt(inewmax));
    testing = [testing mag_presum(1:1200)];

    end

    st=1;
    test2 = zeros(1,1200);

% Adding each 120000 array for integrations
% -----

    for yy = 1:rr,

        tt = testing(st:(st+1199));

        st=st+1200;

        test2 = tt + test2;

    end

% Taking the average
% -----

    ttt = test2/rr;

% Averaged array power

    power_presum = (ttt.*ttt) ;           % [W]
    pres_fft_db = 10*log10(power_presum); % [dB]

```

```

% Setting a variable to Only plot the section of interest
% -----

    Nplot = 1200;

% Calling the use of another program to read the SNR of the
% signal
% -----

    SNR_chirp2

% Setting the max and min for plotting axes
% -----

    mm = 10*log10(max_mag);

    if mm > -95,
        ymax = (round(mm + 5));

    else
        ymax = -95;

    end

    ymin = noise_in_dB - 10;

% Plotting the signal
% -----

figure(4);
plot(Fnew(1:Nplot)*1e-6,pres_fft_db(1:Nplot));grid
axis([0 Fnew(Nplot)*1e-6 ymin ymax])
title('Detected Signal after Dechirping')
xlabel('Frequency (MHz)')
ylabel('Signal (dB)')
aa = sprintf('LO Power: %4.2f dBm',Pwr_lo_dBm);
text(65,-103,aa)
bb = sprintf('Number of spectral averages: %2.0f', rr);
text(65,-106,bb)
cc = sprintf('BW: %2.0f MHz', bandwidth/1e6);
text(65,-109,cc)
dd = sprintf('Pulse duration: %2.0f us', pulsewidth/1e-6);
text(65,-112,dd)
ee = sprintf('Input signal power: %2.0f dBm', pwr_in_dBm);
text(65,-115,ee)
ff = sprintf('Output SNR: %4.2f dB', SNR_dB2);
text(65,-118,ff)

```